ELSEVIER

J. Non-Newtonian Fluid Mech. 141 (2007) 43–58

Journal of Non-Newtonian Fluid Mechanics

www.elsevier.com/locate/jnnfm

Suppression or enhancement of interfacial instability in two-layer plane Couette flow of FENE-P fluids past a deformable solid layer

Janakiramulu Adepu, V. Shankar*

Department of Chemical Engineering, Indian Institute of Technology, Kanpur 208016, India

Received 21 June 2006; received in revised form 26 August 2006; accepted 28 August 2006

Abstract

The linear stability of two-layer plane Couette flow of FENE-P fluids past a deformable solid layer is analyzed in order to examine the effect of solid deformability on the interfacial instability due to elasticity and viscosity stratification at the two-fluid interface. The solid layer is modeled using both linear viscoelastic and neo-Hookean constitutive equations. The limiting case of two-layer flow of upper-convected Maxwell (UCM) fluids is used as a starting point, and results for the FENE-P case are obtained by numerically continuing the UCM results for the interfacial mode to finite values of the chain extensibility parameter. For the case of two-layer plane Couette flow past a rigid solid surface, our results show that the finite extensibility of the polymer chain significantly alters the neutral stability boundaries of the interfacial instability. In particular, the two-layer Couette flow of FENE-P fluids is found to be unstable in a larger range of nondimensional parameters when compared to two-layer flow of UCM fluids. The presence of the deformable solid layer is shown to completely suppress the interfacial instability in most of the parameter regimes where the interfacial mode is unstable, while it could have a completely destabilizing effect in other parameter regimes even when the interfacial mode is stable in rigid channels. When compared with two-layer UCM flow, the two-layer FENE-P case is found in general to require solid layers with relatively lower shear modulii in order to suppress the interfacial instability. The results from the linear elastic solid model are compared with those obtained using the (more rigorous) neo-Hookean model for the solid, and good agreement is found between the two models for neutral stability curves pertaining to the two-fluid interfacial mode. The present study thus provides an important extension of the earlier analysis of two-layer UCM flow [V. Shankar, Stability of two-layer viscoelastic plane Couette flow past a deformable solid layer: implications of fluid viscosity stratification, J. Non-Newtonian Fluid Mech. 125 (2005) 143–158] to more accurate constitutive models for the fluid and solid layers, and reaffirms the central conclusion of instability suppression in two-layer flows of viscoelastic fluids by soft elastomeric coatings in more realistic settings.

Keywords: Interfacial instability; Viscoelastic fluids; Two-layer flows; Linear stability analysis

1. Introduction

Two-layer and multi-layer flows of viscoelastic liquids are known to be prone to interfacial instabilities [1–13] driven by elasticity and viscosity contrasts between the different liquids, and these instabilities often arise during polymer processing operations such as co-extrusion of polymer melts. Such instabilities during melt processing have an adverse impact on the quality (e.g. mechanical and/or optical properties) of the final product, and a clear knowledge of when this instability occurs and how it can be controlled is critical in the design of these operations. Recently, the possibility of suppressing such interfacial instabilities in viscoelastic liquids using soft elastomeric solid coatings was explored by Shankar [14,15]. These studies used the upper-convected Maxwell (UCM) model [16,17] to describe the fluid rheology, and the linear viscoelastic model [18] to describe the solid deformation. Using these relatively simple rheological descriptions for the fluid and solid layers, these studies have shown that it is possible to suppress the interfacial instability driven by elasticity and viscosity stratification under appropriate conditions, when the solid layer becomes sufficiently deformable. In a slightly different context, a recent experimental study by Kulikov and Hornung [19] has shown that rubber coatings can be used to suppress melt fracture, which is a surface defect that occurs even in single-layer processing of molten polymers. If the predicted suppression of *interfacial instabilities* by deformable elastomeric coatings is to be similarly realized in experiments, it

* Corresponding author. Tel.: +91 512 259 7377; fax: +91 512 259 0104.
E-mail address: vshankar@iitk.ac.in (V. Shankar).
URL: http://www.iitk.ac.in/che/vs.htm.

0377-0257/$ – see front matter © 2006 Elsevier B.V. All rights reserved.
doi:10.1016/j.jnnfm.2006.08.011

Nomenclature

b	square of non-dimensional maximum extensibility
c	complex wave-speed ($= c_r + ic_i$)
G	shear modulus of the solid
H	nondimensional thickness of the solid
k	wavenumber
R	dimensional total thickness of the two fluids
V	dimensional velocity of the top plate
W_α	Weissenberg number of fluid α ($= \lambda_\alpha V/R$)

Greek letters

β	nondimensional thickness of fluid 2
$(1-\beta)$	nondimensional thickness of fluid 1
Γ	nondimensional elasticity parameter of solid ($= V\mu_{b0}/GR$)
η_r	ratio of solid to fluid B zero-shear viscosity ($= \eta_w/\mu_{b0}$)
η_w	viscosity of the solid layer
λ_α	relaxation time of fluid α
μ_{a0}	zero-shear viscosity of fluid A
μ_{b0}	zero-shear viscosity of fluid B
μ_r	ratio of zero-shear fluid viscosities ($= \mu_{a0}/\mu_{b0}$)
Σ	nondimensional fluid–fluid interfacial tension ($= \gamma^*/\mu_{b0}V$)

is necessary to extend the previous studies to more accurate constitutive models, both for the fluid and solid layers. The objective of the present work is to carry out such a study by considering the finitely extensible nonlinear elastic-Peterlin (FENE-P) model [16,17] for the viscoelastic liquids, and the neo-Hookean model [20,21] for the deformable solid layer. The FENE-P model accurately captures the shear-rate dependence of shear viscosity as well as the first normal stress difference of polymeric liquids [22], while the neo-Hookean model is a generalization of Hooke's law of elasticity to finite deformations in the solid. The main question the present study sets out to address is whether the predicted suppression of the interfacial instability using simple rheological models remains true for these more accurate constitutive relations for the fluid and the solid layers. In the remainder of this section, relevant literature in related areas is briefly reviewed in order to place the present work in perspective.

Renardy [1] and Chen [2] first predicted the interfacial instability due to elasticity stratification in two-layer plane Couette flow of UCM fluids, respectively, in the short-wave and long-wave limits. They identified the discontinuity in the first normal stress difference in the base state as the primary driving force for the interfacial instability, which could happen in the absence of any viscosity difference between the two fluids, and even in the absence of fluid inertia (i.e. creeping-flow limit). Su and Khomami [3,4] predicted a similar purely elastic interfacial instability for plane Poiseuille flow, and also demonstrated using a pseudospectral method that the interfacial instability occurs for disturbances with arbitrary wavelengths. These early studies employed simple rheological equations for the viscoelastic liquids such as the UCM and Oldroyd-B models, and demonstrated how the instability is controlled by the viscosity ratio, elasticity ratio and the ratio of layer thickness of the two viscoelastic liquids. For the special case of matched fluid viscosities in the two UCM fluids, these studies show that the interface is unstable (stable) in the long-wave limit when the thickness of the more elastic fluid is smaller (larger) than that of the less elastic fluid.

A series of experimental studies has been carried out by Wilson and Khomami [5–8] who provided experimental evidence for the purely elastic interfacial instability in viscoelastic liquids. Ganpule and Khomami [11] have used more realistic constitutive models in order to achieve quantitative agreement with the experimental results. They have employed (i) a modified Oldroyd-B model wherein the shear-rate dependence of first normal stress and the viscosity was incorporated in the classical Oldroyd-B model, which is then equivalent to the White–Metzner model; (ii) a modified Phan–Thien–Tanner model with one relaxation time to accurately capture the steady-shear properties; and (iii) a Giesekus model with both single mode relaxation and multiple mode relaxation. They concluded that the multimode Giesekus model can quantitatively describe the interfacial instability in terms of both neutral stability curves as well as growth rates. They also presented a detailed and rigorous energy budget of the disturbance energies, and provided a mechanistic insight for the interfacial instability. More recently, Valette et al. [13] have carried out experimental and theoretical studies for two-layer plane Poiseuille flow of polyethylene and polystyrene melts, and showed that the White–Metzner constitutive relation is able to account for the spatial amplification rate measured form experiments. The White–Metzner model is a generalization of the UCM/Oldroyd-B class of models which phenomenologically incorporates a shear-rate-dependent relaxation time (i.e. first normal stress difference), and a shear-rate-dependent viscosity of the Carreau–Yasuda type. In this study, we describe the viscoelastic liquids using the FENE-P model, which describes a polymer chain as a dumbell of two beads (which act as centers of hydrodynamic resistance) connected by an entropic spring, which has finite extensibility. Albeit being more complicated, the FENE-P constitutive relation has a rigorous molecular basis, and has been extensively used to correlate experimental data for various dynamical properties of polymer solutions such as shear and extensional viscosities, transients and normal stress differences [23].

The effect of a deformable solid layer coating on the two-fluid interfacial instability due to elasticity and/or viscosity stratification was recently analyzed [14,15]. These studies employed the UCM model for the viscoelastic liquids and the linear viscoelastic model for the deformable solid. It was shown using long-wave asymptotic analysis and a numerical method that, under appropriate conditions, the two-fluid interfacial instability can be completely suppressed at all wavenumbers when the solid layer becomes sufficiently deformable. Under conditions when the two-fluid mode is stable, it was shown that the solid layer could even destabilize the interfacial mode. However, these studies have employed relatively simple descriptions for the con-

stitutive nature of the fluids and the solid. The UCM model has the limitation that the viscosity and the first normal stress are independent of the shear rate which are overcome in the FENE-P constitutive relation. Since the interfacial instability in viscoelastic liquids is critically dependent on normal stress difference, one may expect the results obtained from the FENE-P model to be significantly different owing to the shear-rate dependent normal stress difference. Furthermore, the linear viscoelastic solid model employed in the previous studies [14,15] is strictly valid only when the nondimensional strain in the solid is small compared to one. In a recent series of papers, Gkanis and Kumar [24–26] employed the neo-Hookean model for the deformable solid and showed that there could be significant differences between the predictions of the two models, especially in the presence of another interface in addition to the liquid–solid interface, similar to one encountered in the present study. The neo-Hookean solid is a rigorous generalization of the Hookean elastic solid to finite deformations [20,21], and exhibits a first normal stress difference under simple shear deformation. Gkanis and Kumar [24] showed that for Newtonian fluid flow (which does not posses any normal stress difference under simple shear) past a neo-Hookean solid, this additional normal stress difference in the solid gives rise to an interfacial instability at high wavenumbers, much akin to the two-fluid instability in viscoelastic liquids. In view of these recent findings by Gkanis and Kumar, it is of interest here to critically evaluate and extend the previous results [14,15] obtained using the linear elastic model to the neo-Hookean case in order to verify whether there are qualitative differences in the prediction of instability suppression, or if the differences are merely quantitative.

The rest of the paper is organized as follows: the fundamental governing equations for the FENE-P fluids and the deformable solid are outlined in Section 2.1, and the base-state velocity and stress profiles are given in Section 2.2. The linearized governing equations and boundary conditions for the stability problem are discussed in Section 2.3, while the numerical methodology used for solving the stability problem is outlined in Section 3. In Section 4.1, we provide new results for the stability of two-layer flow of FENE-P fluids in rigid channels, and demonstrate how the neutral stability boundaries are significantly altered. The results discussed in this part of the paper augment the current literature on instability due to elasticity stratification for two-layer viscoelastic flows in rigid channels. Section 4.2 discusses the comparison of results obtained from UCM and FENE-P fluids for the effect of the deformable solid layer on the interfacial mode. The comparison between results from the neo-Hookean solid model and linear elastic solid are provided in Section 4.3. The salient conclusions of the present study are summarized in Section 5.

2. Problem formulation

2.1. Governing equations

The system under consideration (see Fig. 1) consists of a deformable solid of thickness HR, shear modulus G, fixed onto a rigid surface at $z^* = -HR$, a layer of viscoelastic fluid (fluid B) of thickness βR in the region $0 < z^* < \beta R$ with zero-shear viscosity μ_{b0}, relaxation time λ_b, and another viscoelastic fluid layer (fluid A) of thickness $(1-\beta)R$ in the region $\beta R < z^* < R$ with zero-shear viscosity μ_{a0}, relaxation time λ_a. The two viscoelastic fluids are modeled in this work using the FENE-P model (see, for example, [16,17,22,27]), details of which are presented below. The densities of the two fluids are assumed to be the same ($\rho_a = \rho_b = \rho$), in order to exclusively focus on the instability of the two-fluid interface due to elasticity and viscosity stratification. In what follows, we indicate dimensional variables with a superscript *, and nondimensional variables without any superscript. Fluid A is bounded at $z^* = R$ by a rigid wall which moves at a constant velocity V in the x-direction relative to the deformable solid layer. The following scales are used for nondimensionalising various physical quantities in this work: R for lengths and displacements, V for velocities, R/V for time, and $\mu_{b0}V/R$ for stresses and pressure. H, therefore, is the nondimensional thickness of the solid layer, while $(1-\beta)$ and β are respectively the nondimensional thickness of fluids A and B.

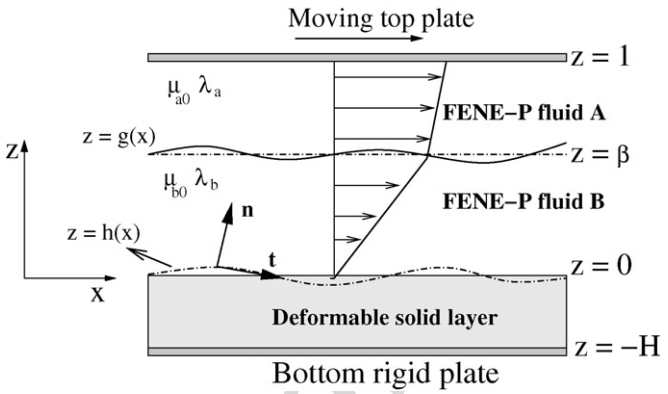

Fig. 1. Schematic diagram showing the configuration and (nondimensional) coordinate system considered in Section 2. Two FENE-P fluids with zero-shear viscosities μ_{a0} and μ_{b0}, and with relaxation times λ_a and λ_b flowing past a deformable solid layer.

2.1.1. FENE-P fluids

The constitutive model used in this work for describing the two viscoelastic liquids is the FENE-P dumbell model, in which a polymer molecule is represented by a dumbell consisting of two beads which act as the source of hydrodynamic resistance, connected by a finitely extensible 'spring' which represents the entropic elasticity of a single polymer molecule [16,17,22]. For simplicity, we assume no solvent contribution to the stress in the polymeric liquid, thereby restricting our attention to polymer melts. The solvent contribution to the stress tensor, even if included, will weaken the first normal stress difference in the fluid, which is the primary driving force for the interfacial instability. In the FENE-P model, the viscoelastic stress (extra stress tensor) $\boldsymbol{\tau}^\alpha$ in the polymeric liquid is given in terms of the polymer chain conformation tensor $\mathbf{c}$ as

$$\boldsymbol{\tau}^\alpha = \mu_r^\alpha \frac{f^\alpha(\mathbf{Q})\mathbf{c}^\alpha - \mathbf{I}}{W_\alpha}, \tag{1}$$

where $\mathbf{c}$ is the nondimensional conformation tensor characterizing the average second moment of the end-to-end vector $\mathbf{Q}$ of the polymer molecule, and $\mathbf{c}$ reduces to the identity tensor $\mathbf{I}$ at equilibrium. The superscript α represents fluid labels a and b. Here, the ratio of the zero-shear viscosities in the two fluids is denoted by $\mu_{\mathrm{r}}^{\mathrm{a}} = \mu_{\mathrm{a0}}/\mu_{\mathrm{b0}} \equiv \mu_{\mathrm{r}}$ for $\alpha = a$, and $\mu_{\mathrm{r}}^{\mathrm{b}} = \mu_{\mathrm{b0}}/\mu_{\mathrm{b0}} = 1$ for $\alpha = b$. The Weissenberg number in fluid α, $W_\alpha \equiv \lambda_\alpha V/R$, denotes the dimensionless relaxation time in fluid α. The dimensional group used for nondimensionalising the conformation tensor is $k_{\mathrm{B}}T/H_{\mathrm{spring}}$, where H_{spring} is the spring constant of the dumbbell, k_{B} the Boltzmann constant and T is the absolute temperature. The term $f^\alpha(\mathbf{Q})$ is the Peterlin function, given by

$$f^\alpha = \frac{b^\alpha - 3}{b^\alpha - \mathrm{trace}(\mathbf{c}^\alpha)}, \tag{2}$$

where b^α is the square of the nondimensional maximum extensibility of the dumbbell, and clearly $\mathrm{trace}(\mathbf{c}) \leq b$. The quantity b has also been nondimensionalized using $k_{\mathrm{B}}T/H_{\mathrm{spring}}$. The parameter b, then, denotes the finite extensibility of the chain, and it typically ranges between 10 and 100 [17], and the limit $b \to \infty$ represents the limit of an infinitely extensible chain where the FENE-P constitutive relation reduces to the upper-convected Maxwell (UCM) model.

The time-evolution of the conformation tensor $\mathbf{c}^\alpha$ is governed by

$$\partial_t \mathbf{c}^\alpha + \mathbf{v}^\alpha \cdot (\nabla \mathbf{c}^\alpha) - [\mathbf{c}^\alpha \cdot (\nabla \mathbf{v}^\alpha) + (\nabla \mathbf{v}^\alpha)^{\mathrm{T}} \cdot \mathbf{c}^\alpha] = -\left(\frac{f^\alpha \mathbf{c}^\alpha - \mathbf{I}}{W_\alpha}\right). \tag{3}$$

Under simple shear flow, the FENE-P model predicts a shear-rate dependent viscosity μ and a shear-rate dependent first normal stress difference. The nondimensional equations governing the dynamics of the two fluids are respectively the continuity and momentum conservation equations:

$$\nabla \cdot \mathbf{v}^\alpha = 0, \qquad Re[\partial_t + \mathbf{v}^\alpha \cdot \nabla]\mathbf{v}^\alpha = \nabla \cdot \mathbf{T}^\alpha. \tag{4}$$

Here, $\mathbf{v}^\alpha$ is the velocity field in fluid α, and $\mathbf{T}^\alpha = -p^\alpha \mathbf{I} + \boldsymbol{\tau}^\alpha$ the total stress tensor in fluid α which is a sum of an isotropic pressure contribution and the extra-stress tensor $\boldsymbol{\tau}^\alpha$. In the above equation, $Re = \rho VR/\mu_{\mathrm{b0}}$ is the Reynolds number based on the zero-shear viscosity of fluid B. No-slip boundary conditions are appropriate for fluid A at $z = 1$:

$$v_x^{\mathrm{a}} = 1, \qquad v_z^{\mathrm{a}} = 0, \tag{5}$$

while the boundary conditions at the interface between the two FENE-P fluids A and B and the interface between the fluid B and the solid layer are the continuity of velocity and stresses. At the interface between the two fluids $z = g(x)$, we therefore have

$$\mathbf{v}^{\mathrm{a}} = \mathbf{v}^{\mathrm{b}}, \qquad \mathbf{T}^{\mathrm{b}} \cdot \mathbf{n} = \mathbf{T}^{\mathrm{a}} \cdot \mathbf{n} + \mathbf{n}\kappa\Sigma, \tag{6}$$

where κ is the mean curvature of the fluid–fluid interface, $\mathbf{n}$ the unit vector to the two-fluid interface pointing into fluid A, and $\Sigma \equiv \gamma^*/(\mu_{\mathrm{b0}}V)$ is the nondimensional interfacial tension of the liquid–liquid interface. The interface conditions are supplemented by the kinematic condition for the evolution of the interfacial position $g(x)$.

2.1.2. Linear viscoelastic solid

In this study, the deformable solid layer is modeled using both a simple linear viscoelastic solid model [14,15,28] and the neo-Hookean solid model [24–26]. While most of the earlier studies in the area of fluid flow past deformable solid surfaces had employed the linear viscoelastic solid model, in a recent series of papers, Gkanis and Kumar [24–26] have pointed out the importance of using the neo-Hookean solid model to describe the solid deformation. The linear viscoelastic solid model is readily amenable to mathematical analysis and also allows for incorporation of viscous dissipative effects in the solid in a relatively simple way. However, it has the drawback that, strictly speaking, it is valid only in the limit of small strains in the deformable solid. The neo-Hookean solid, which is a generalization of the linear elastic solid to large (i.e. finite) deformations, has been used to describe the behaviour of model elastomers [21], and it successfully overcomes the limitations of the linear elastic solid model. In this study, we use both these models with the objective of evaluating the predictions of the two models in the context of the effect of solid deformability on the interfacial instability.

In the linear viscoelastic solid, the dynamics of the solid layer is described by a displacement field $\mathbf{u}$, which represents the displacement of the material points in the medium from their steady-state positions. The velocity field in the solid layer is $\mathbf{v} = \partial_t \mathbf{u}$. In an incompressible linear viscoelastic solid, the displacement field satisfies the continuity equation:

$$\nabla \cdot \mathbf{u} = 0. \tag{7}$$

The momentum conservation equation in the solid is given by

$$Re\, \partial_t^2 \mathbf{u} = \nabla \cdot \boldsymbol{\Pi}, \tag{8}$$

where $\boldsymbol{\Pi} = -p_{\mathrm{g}}\mathbf{I} + \boldsymbol{\sigma}$ is the total stress tensor which is given by a sum of the isotropic pressure and the deviatoric stress $\boldsymbol{\sigma}$. Without loss of generality, it is assumed here that the density of the solid is equal to the density of the two fluids. The deviatoric stress tensor $\boldsymbol{\sigma}$ is given by a sum of elastic and viscous stresses in the solid layer:

$$\boldsymbol{\sigma} = \left(\frac{1}{\Gamma} + \eta_{\mathrm{r}}\partial_t\right)(\nabla \mathbf{u} + (\nabla \mathbf{u})^{\mathrm{T}}), \tag{9}$$

where $\Gamma = V\mu_{\mathrm{b0}}/(GR)$ is the nondimensional quantity characterizing the elasticity of the solid layer and $\eta_{\mathrm{r}} = \eta_{\mathrm{w}}/\mu_{\mathrm{b0}}$ is the ratio of solid viscosity and zero-shear viscosity of fluid B. More precisely, $1/\Gamma$ is the estimated ratio of elastic stresses in the solid layer to viscous stresses in fluid B. As we will show below, the strain in the solid in the base state is also proportional to Γ, and one would expect the linear viscoelastic model to be accurate if $\Gamma \ll 1$ in the problem of interest. In the earlier study by one of the authors [15] for two-layer flow of UCM fluids, it was indeed found that the Γ required for stabilizing the interfacial instability is significantly lesser than unity. We arrive at a similar conclusion later in our discussion for FENE-P fluids, thereby justifying use of the linear viscoelastic model for the present purposes.

The solid layer is assumed to be fixed to a rigid surface at $z = -H$, and the boundary condition for the displacement

field there is $\mathbf{u} = 0$. The boundary conditions at the fluid B–solid interface $z = h(x)$ are the continuity of velocities and stresses at this interface, and these conditions are presented in the context of the neo-Hookean solid in the following subsection.

2.1.3. Neo-Hookean solid

In the neo-Hookean solid model [20,21,24], the fundamental quantity describing the deformation is the deformation tensor $\mathbf{F}$, which is defined as

$$\mathbf{F} = \nabla_X \mathbf{w}. \tag{10}$$

Here, and in the following discussion for the neo-Hookean solid, $\mathbf{X}$ represents the position vector in the reference configuration, and $\mathbf{w} = \mathbf{w}(\mathbf{X}, t)$ is the position vector in the current configuration. We adopt the convention similar to one used by Gkanis and Kumar [24], and let $\mathbf{X} = (X, Y, Z)$ when we describe the solid deformation, and ∇_X is the gradient operator in terms of the reference coordinates. This reference coordinate system coincides with the Cartesian (x, y, z) coordinate system used to describe the variation of dynamical quantities in the fluid. Without loss of generality, we consider the case of the neo-Hookean model in the zero-inertia limit, and since the densities of the fluids and the deformable solid are comparable, this would imply that we must consider the dynamics of the two fluids also in the zero-inertia/creeping-flow limit. Under these conditions, the equations describing the deformation in the neo-Hookean solid are given as follows. The mass conservation equation for an incompressible neo-Hookean solid is given by [20]:

$$\det(\mathbf{F}) = 1 \tag{11}$$

and the momentum conservation equation is given by

$$\nabla_X \cdot \mathbf{P} = 0, \tag{12}$$

where $\mathbf{P}$ is the first Piola-Kirchhoff stress tensor [20], which is related to the Cauchy stress tensor $\boldsymbol{\sigma}$ through the equation $\mathbf{P} = \mathbf{F}^{-1} \cdot \boldsymbol{\sigma}$. The neo-Hookean constitutive relation prescribes the Cauchy stress tensor as

$$\boldsymbol{\sigma} = -p_g \mathbf{I} + \frac{1}{\Gamma} \mathbf{F} \cdot \mathbf{F}^{\mathrm{T}}. \tag{13}$$

The boundary condition for the neo-Hookean solid at the bottom rigid surface at $z = -H$ is the zero displacement condition given by $\mathbf{w} = \mathbf{X}$. At the interface $z = h(x)$ between fluid B and the deformable solid layer, we have the velocity continuity condition:

$$\mathbf{v} = \partial_t \mathbf{u}, \qquad \text{for linear viscoelastic solid,} \tag{14}$$

$$\mathbf{v} = \partial_t \mathbf{w}, \qquad \text{for neo-Hookean solid,} \tag{15}$$

and the stress balance at the fluid B–solid interface is given by

$$\mathbf{n} \cdot \boldsymbol{\sigma} = \mathbf{n} \cdot \boldsymbol{\tau}. \tag{16}$$

The interfacial tension at the liquid–solid interface is neglected in this study.

2.2. Base state

2.2.1. FENE-P fluids

The steady, unidirectional, x-independent base state, whose stability is under discussion, is obtained by solving the momentum equations in fluids A and B. We look for a steady solution in which the fluid–fluid interface is flat and uniform, and the unit normal to this interface is given by $\mathbf{n} = (0, 0, 1)$, and the unit tangent vector to this interface is $\mathbf{t} = (1, 0, 0)$.

We first outline the key steps in deriving the base state velocity profiles in the two FENE-P fluids. The x-momentum equation simplifies under the above assumptions to

$$\mathrm{d}_z \bar{\tau}^{\alpha}_{xz} = 0, \tag{17}$$

where $\mathrm{d}_z = \mathrm{d}/\mathrm{d}z$, and this yields $\bar{\tau}^{\alpha}_{xz} =$ constant independent of z in each fluid. From the expression for the stress tensor for FENE-P fluids (1), we obtain

$$\bar{\tau}^{\alpha}_{xz} = \frac{\mu^{\alpha}_{\mathrm{r}} \bar{f}^{\alpha} \bar{c}^{\alpha}_{xz}}{W_{\alpha}}, \qquad \bar{\tau}^{\alpha}_{xx} = \mu^{\alpha}_{\mathrm{r}} \frac{\bar{f}^{\alpha} \bar{c}^{\alpha}_{xx} - 1}{W_{\alpha}},$$
$$\bar{\tau}^{\alpha}_{zz} = \mu^{\alpha}_{\mathrm{r}} \frac{\bar{f}^{\alpha} \bar{c}^{\alpha}_{zz} - 1}{W_{\alpha}}, \tag{18}$$

where

$$\bar{f}^{\alpha} = \frac{b^{\alpha} - 3}{b^{\alpha} - (\bar{c}^{\alpha}_{xx} + \bar{c}^{\alpha}_{yy} + \bar{c}^{\alpha}_{zz})}. \tag{19}$$

Using the evolution equation (3) for the conformation tensor $\mathbf{c}$, we obtain under the base-state flow assumptions:

$$\bar{c}^{\alpha}_{xz} = \frac{W_{\alpha} \bar{c}^{\alpha}_{zz}}{\bar{f}^{\alpha}} \mathrm{d}_z \bar{v}^{\alpha}_x, \qquad 2\bar{c}^{\alpha}_{xz} \mathrm{d}_z \bar{v}^{\alpha}_x = \frac{\bar{f}^{\alpha} \bar{c}^{\alpha}_{xx} - 1}{W_{\alpha}},$$
$$\bar{c}^{\alpha}_{zz} = \bar{c}^{\alpha}_{yy} = \frac{1}{\bar{f}^{\alpha}}. \tag{20}$$

By substituting Eq. (20) in Eq. (18), we obtain

$$\bar{\tau}^{\alpha}_{xz} = \mu^{\alpha}_{\mathrm{r}} \bar{c}^{\alpha}_{zz} \mathrm{d}_z \bar{v}^{\alpha}_x. \tag{21}$$

Substituting this in Eq. (17), and postulating that $\bar{c}^{\alpha}_{zz}$ is independent of z (as will be demonstrated a little later that), we obtain linear velocity profiles in both the FENE-P fluids:

$$\bar{v}^{\mathrm{a}}_x = B_1 z + B_2, \quad \bar{v}^{\mathrm{b}}_x = D_1 z + D_2. \tag{22}$$

The conditions to be used to solve for the constants are the no-slip conditions at $z = 1$, $\bar{v}^{\mathrm{a}}_x = 1$ and at $z = 0$, $\bar{v}^{\mathrm{b}}_x = 0$; and continuity conditions $\bar{v}^{\mathrm{a}}_x = \bar{v}^{\mathrm{b}}_x$ and $\bar{\tau}^{\mathrm{a}}_{xz} = \bar{\tau}^{\mathrm{b}}_{xz}$ at the unperturbed interface $z = \beta$. After solving for the constants, we obtain

$$\bar{v}^{\mathrm{a}}_x = \frac{z + \beta((\mu_{\mathrm{r}}/\bar{f}_{\mathrm{r}}) - 1)}{1 + \beta((\mu_{\mathrm{r}}/\bar{f}_{\mathrm{r}}) - 1)}, \qquad \bar{v}^{\mathrm{a}}_z = 0, \tag{23}$$

$$\bar{\tau}^{\mathrm{a}}_{xx} = \frac{2\mu_{\mathrm{r}} W_a \bar{c}^{\mathrm{a}}_{zz} \bar{c}^{\mathrm{a}}_{zz}}{[1 + \beta((\mu_{\mathrm{r}}/\bar{f}_{\mathrm{r}}) - 1)]^2}, \qquad \bar{\tau}^{\mathrm{a}}_{zz} = 0,$$
$$\bar{\tau}^{\mathrm{a}}_{xz} = \bar{\tau}^{\mathrm{a}}_{zx} = \frac{\mu_{\mathrm{r}} \bar{c}^{\mathrm{a}}_{zz}}{1 + \beta((\mu_{\mathrm{r}}/\bar{f}_{\mathrm{r}}) - 1)}, \tag{24}$$

$$\bar{v}^{\mathrm{b}}_x = \frac{\mu_{\mathrm{r}} z}{\bar{f}_{\mathrm{r}}[1 + \beta((\mu_{\mathrm{r}}/\bar{f}_{\mathrm{r}}) - 1)]}, \qquad \bar{v}^{\mathrm{b}}_z = 0, \tag{25}$$

$$\bar{\tau}^{\mathrm{b}}_{xx} = \frac{2W_{\mathrm{b}}(\mu_{\mathrm{r}}\bar{c}^{\mathrm{a}}_{zz})^2}{[1+\beta((\mu_{\mathrm{r}}/\bar{f}_{\mathrm{r}})-1)]^2}, \qquad \bar{\tau}^{\mathrm{b}}_{zz} = 0, \qquad \bar{\tau}^{\mathrm{b}}_{xz} = \bar{\tau}^{\mathrm{a}}_{xz}. \tag{26}$$

In the above equations, $\bar{f}_{\mathrm{r}} \equiv \bar{f}^{\mathrm{a}}/\bar{f}^{\mathrm{b}}$, and these are computed as discussed below. Note that the nonzero first normal stress difference $\bar{\tau}^{(\alpha)}_{xx} - \bar{\tau}^{(\alpha)}_{zz}$ ($\alpha = \mathrm{a}, \mathrm{b}$) is different in the two fluids, and it is discontinuous across the two-fluid interface.

The determination of the velocity and stress profiles in the fluids involves the knowledge of $\bar{f}^{\mathrm{a}}$ and $\bar{f}^{\mathrm{b}}$, which in turn depend on the components $\bar{c}^{\alpha}_{zz}$, $\bar{c}^{\alpha}_{xx}$ and $\bar{c}^{\alpha}_{xz}$ of the conformation tensor in the two fluids. These are obtained from the evolution equations for the conformation tensor in the base state, which are coupled nonlinear set of equations. We solve them using a Newton–Raphson iteration scheme to obtain the base state components of the conformation tensor in the two fluids. The coupled set of equations for $\bar{c}^{\alpha}_{ij}$ are independent of the normal coordinate z, and so the components themselves are z-independent quantities.

The velocity profile in the two FENE-P fluids is linear in z, and there is a first normal stress difference in the two fluids which vanishes only when $W_\alpha = 0$. The first normal stress difference is a shear-rate-dependent quantity in a FENE-P fluid. In the case of FENE-P fluids with matched zero-shear viscosities $\mu_{\mathrm{r}} = 1$, but with different W_a and W_{b} (i.e. different relaxation times), there will still be a discontinuity in the gradient of the velocity at the interface. This is in contrast to the two-layer UCM case, because for FENE-P fluids with identical zero-shear viscosities, but different relaxation times, the shear thinning is different in the two fluids leading to different effective viscosities at higher shear rates. Mathematically, this can been seen from Eqs. (23) and (25), where even if $\mu_{\mathrm{r}} = 1$, $\bar{f}_{\mathrm{r}} \neq 1$ for $W_{\mathrm{a}} \neq W_{\mathrm{b}}$ and so there will be a slope discontinuity in the base-state velocity profile at the interface. The shear-rate dependent viscosity is obtained by dividing the shear stress with the actual shear rate, and the ratio of shear-rate dependent viscosity to the zero-shear viscosity is simply given by $\bar{\tau}_{xz}$.

2.2.2. Deformable solid layer

We next discuss the base state displacement and stresses in both the linear viscoelastic and the neo-Hookean model.

The solid layer is at rest in this steady base state, but there is a nonzero unidirectional displacement $\bar{u}_x$ due to the fluid shear stresses at the interface:

$$\bar{u}_x = \frac{\Gamma(z+H)}{\bar{f}^{\mathrm{b}}}\,\mathrm{d}_z\bar{v}^{\mathrm{b}}_x, \qquad \bar{u}_z = 0, \qquad \bar{\sigma}_{xx} = 0, \qquad \bar{\sigma}_{zz} = 0, \tag{27}$$

$$\bar{\sigma}_{xz} = \bar{\sigma}_{zx} = \frac{\mathrm{d}_z\bar{v}^{\mathrm{b}}_x}{\bar{f}^{\mathrm{b}}}. \tag{28}$$

Note that the tangential displacement in the base state is a function of W_α through the terms $\mathrm{d}_z\bar{v}^{\mathrm{b}}_x$ and $\bar{f}^{\mathrm{b}}$ in the above equation. In the linear viscoelastic solid layer, the first normal stress difference is identically zero.

In the neo-Hookean solid, the base state quantities are obtained as follows

$$\bar{w}_X = X + \frac{\Gamma(Z+H)}{\bar{f}^{\mathrm{b}}}\mathrm{d}_z\bar{v}^{\mathrm{b}}_x, \qquad \bar{w}_Z = Z,$$
$$C_1 \equiv \mathrm{d}_z\bar{w}_X = \frac{\Gamma}{\bar{f}^{\mathrm{b}}}\mathrm{d}_z\bar{v}^{\mathrm{b}}_x. \tag{29}$$

The components of the Cauchy stress tensor in the base state of the neo-Hookean solid are given by

$$\bar{\sigma}_{XX} = -\bar{p}_{\mathrm{g}} + \frac{1+C_1^2}{\Gamma}, \quad \bar{\sigma}_{YY} = \bar{\sigma}_{ZZ} = -\bar{p}_{\mathrm{g}} + \frac{1}{\Gamma},$$
$$\bar{\sigma}_{XZ} = \bar{\sigma}_{ZX} = \frac{C_1}{\Gamma}. \tag{30}$$

Here, C_1 is the tangential displacement gradient in the solid, and this depends on W_α. The neo-Hookean solid exhibits a first normal stress difference under simple shear, and $\bar{\sigma}_{XX} - \bar{\sigma}_{ZZ} = C_1^2/\Gamma$ in the solid. All the base flow quantities above are denoted with an overbar in the preceding and ensuing discussions.

2.3. Linear stability analysis

A temporal stability analysis is employed to determine the stability of small perturbations to the above base state. Small, two-dimensional perturbations (denoted by primed quantities) are introduced to all dynamical quantities about their base state values, e.g. $v^{\alpha}_i = \bar{v}^{\alpha}_i + v^{\alpha'}_i$. The perturbation quantities are expanded in terms of Fourier modes in the x-direction, and with an exponential time dependence: $v^{\alpha'}_i = \tilde{v}^{\alpha'}_i(z)\exp[\mathrm{i}k(x-ct)]$. Here k is the wavenumber, c is the wavespeed, and $\tilde{v}^{\alpha}_i(z)$ are eigenfunctions which are determined below from the linearized governing equations and boundary conditions. The complex wavespeed $c = c_{\mathrm{r}} + \mathrm{i}c_i$, and when $c_i > 0$, the base state is temporally unstable.

2.3.1. FENE-P fluids

Upon substituting the above form for the perturbations in the governing equations for the two fluids (4) we obtain the following linearized equations for the two fluids, where $\alpha = \mathrm{a}, \mathrm{b}$:

$$\mathrm{d}_z\tilde{v}^{\alpha}_z + \mathrm{i}k\tilde{v}^{\alpha}_x = 0, \tag{31}$$

$$-\mathrm{i}k\tilde{p}^{\alpha} + \mathrm{i}k\tilde{\tau}^{\alpha}_{xx} + \mathrm{d}_z\tilde{\tau}^{\alpha}_{xz} = Re[\mathrm{i}k(\bar{v}^{\alpha}_x - c)\tilde{v}^{\alpha}_x + \mathrm{d}_z\bar{v}^{\alpha}_x\tilde{v}^{\alpha}_z], \tag{32}$$

$$-\mathrm{d}_z\tilde{p}^{\alpha} + \mathrm{d}_z\tilde{\tau}^{\alpha}_{zz} + \mathrm{i}k\tilde{\tau}^{\alpha}_{xz} = Re[\mathrm{i}k(\bar{v}^{\alpha}_x - c)]\tilde{v}^{\alpha}_z. \tag{33}$$

The constitutive relation and the evolution equation for the conformation tensor are similarly linearized for the two FENE-P fluids. For example, the quantity $f^{\alpha} = \bar{f}^{\alpha} + f^{\alpha'}$ is linearized as

$$\bar{f}^{\alpha} + f^{\alpha'} = \frac{b^{\alpha}-3}{b^{\alpha} - \bar{c}^{\alpha}_{xx} - 2\bar{c}^{\alpha}_{zz}} + \frac{(b^{\alpha}-3)(c^{\alpha'}_{xx} + 2c^{\alpha'}_{zz})}{(b^{\alpha} - \bar{c}^{\alpha}_{xx} - 2\bar{c}^{\alpha}_{zz})^2}. \tag{34}$$

The linearized evolution equations for the various components of the conformation tensor $\mathbf{c}$ are given by

$$\left[\mathrm{i}kW_\alpha(\bar{v}_x^\alpha - c) + \frac{\bar{c}_{xx}^\alpha}{(b^\alpha-3)(\bar{c}_{zz}^\alpha)^2} + \frac{1}{\bar{c}_{zz}^\alpha}\right]\tilde{c}_{xx}^\alpha = 2W_\alpha[\mathrm{d}_z\bar{v}_x^\alpha\tilde{c}_{xz}^\alpha + \tilde{c}_{xz}^\alpha\mathrm{d}_z\tilde{v}_x^\alpha + \mathrm{i}k\tilde{c}_{xx}^\alpha\tilde{v}_x^\alpha] - \left(\frac{2\tilde{c}_{zz}^\alpha\bar{c}_{xx}^\alpha}{(b^\alpha-3)(\bar{c}_{zz}^\alpha)^2}\right), \tag{35}$$

$$\left[\mathrm{i}kW_\alpha(\bar{v}_x^\alpha - c) + \frac{2}{(b^\alpha-3)\bar{c}_{zz}^\alpha} + \frac{1}{\bar{c}_{zz}^\alpha}\right]\tilde{c}_{zz}^\alpha = 2\mathrm{i}kW_\alpha\bar{c}_{xz}^\alpha\tilde{v}_z^\alpha + 2W_\alpha\bar{c}_{zz}^\alpha\mathrm{d}_z\tilde{v}_z^\alpha - \left(\frac{\tilde{c}_{xx}^\alpha}{(b^\alpha-3)\bar{c}_{zz}^\alpha}\right), \tag{36}$$

$$\left[\mathrm{i}kW_\alpha(\bar{v}_x^\alpha - c) + \frac{1}{\bar{c}_{zz}^\alpha}\right]\tilde{c}_{xz}^\alpha = \mathrm{i}kW_\alpha\bar{c}_{xx}^\alpha\tilde{v}_z^\alpha + W_\alpha\bar{c}_{zz}^\alpha\mathrm{d}_z\tilde{v}_x^\alpha + W_\alpha\mathrm{d}_z\bar{v}_x^\alpha\tilde{c}_{zz}^\alpha - \left(\frac{\tilde{c}_{xx}^\alpha + 2\tilde{c}_{zz}^\alpha}{(b^\alpha-3)(\bar{c}_{zz}^\alpha)^2}\right)\bar{c}_{xz}^\alpha. \tag{37}$$

The linearized equations for the stress components in the FENE-P fluids are

$$\tilde{\tau}_{xx}^\alpha = \frac{\mu_\mathrm{r}^\alpha}{W_\alpha}\left[\frac{(\tilde{c}_{xx}^\alpha + 2\tilde{c}_{zz}^\alpha)\bar{c}_{xx}^\alpha}{(b^\alpha-3)\bar{c}_{zz}^\alpha\bar{c}_{zz}^\alpha} + \frac{\tilde{c}_{xx}^\alpha}{\bar{c}_{zz}^\alpha}\right], \tag{38}$$

$$\tilde{\tau}_{zz}^\alpha = \frac{\mu_\mathrm{r}^\alpha}{W_\alpha}\left[\frac{(\tilde{c}_{xx}^\alpha + 2\tilde{c}_{zz}^\alpha)}{(b^\alpha-3)\bar{c}_{zz}^\alpha} + \frac{\tilde{c}_{zz}^\alpha}{\bar{c}_{zz}^\alpha}\right], \tag{39}$$

$$\tilde{\tau}_{xz}^\alpha = \frac{\mu_\mathrm{r}^\alpha}{W_\alpha}\left[\frac{(\tilde{c}_{xx}^\alpha + 2\tilde{c}_{zz}^\alpha)\bar{c}_{xz}^\alpha}{(b^\alpha-3)\bar{c}_{zz}^\alpha\bar{c}_{zz}^\alpha} + \frac{\tilde{c}_{xz}^\alpha}{\bar{c}_{zz}^\alpha}\right]. \tag{40}$$

A single fourth-order differential equation for $\tilde{v}_z^\alpha$ can be obtained from Eqs. (31)–(33) to give

$$k(\mathrm{d}_z^2 + k^2)\tilde{\tau}_{xz}^\alpha + \mathrm{i}k^2\mathrm{d}_z(\tilde{\tau}_{xx}^\alpha - \tilde{\tau}_{zz}^\alpha) + Re\,k(\bar{v}_x^\alpha - c)(\mathrm{d}_z^2 - k^2)\tilde{v}_z^\alpha = 0, \tag{41}$$

where the various Fourier components of the linearized stresses must be obtained from Eqs. (38)–(40), and the components of the conformation tensor are obtained from Eqs. (35)–(37).

The linearized boundary conditions at the unperturbed interface position $z = \beta$ between the two FENE-P fluids A and B are obtained by Taylor-expanding about the perturbed interface [1,2]:

$$\tilde{v}_z^\mathrm{a} = \tilde{v}_z^\mathrm{b}, \tag{42}$$

$$\tilde{v}_x^\mathrm{a} + [\mathrm{d}_z\bar{v}_x^\mathrm{a}]_{z=\beta}\,\tilde{g} = \tilde{v}_x^\mathrm{b} + [\mathrm{d}_z\bar{v}_x^\mathrm{b}]_{z=\beta}\,\tilde{g}, \tag{43}$$

$$-\tilde{p}^\mathrm{a} + \tilde{\tau}_{zz}^\mathrm{a} - \Sigma k^2\tilde{g} = -\tilde{p}^\mathrm{b} + \tilde{\tau}_{zz}^\mathrm{b} \tag{44}$$

$$\tilde{\tau}_{xz}^\mathrm{a} - \mathrm{i}k\bar{\tau}_{xx}^\mathrm{a}\tilde{g} = \tilde{\tau}_{xz}^\mathrm{b} - \mathrm{i}k\bar{\tau}_{xx}^\mathrm{b}\tilde{g}, \tag{45}$$

where $\tilde{g}$ is the Fourier expansion coefficient for the interface position $g = \tilde{g}\exp[\mathrm{i}k(x-ct)]$, and $\Sigma = \gamma^*/(\mu_{\mathrm{b}0}V)$ is the nondimensional interfacial tension between fluids A and B. The tangential stress condition (Eq. (45)) has additional terms due to the jump in the first normal stress difference across the two-fluid interface in the base state. These additional terms are responsible for the purely elastic interfacial instability in two-layer flows of viscoelastic fluids. The linearized kinematic condition at $z = \beta$ between the two viscoelastic fluids is given by

$$\mathrm{i}k[\bar{v}_x^\mathrm{a}(z=\beta) - c]\tilde{g} = \tilde{v}_z^\mathrm{a}[z=\beta]. \tag{46}$$

The boundary conditions at $z = 1$ are simply

$$\tilde{v}_z^\mathrm{a} = 0, \qquad \tilde{v}_x^\mathrm{a} = 0. \tag{47}$$

2.3.2. Linear viscoelastic solid

The governing equations for the displacement field in the linear viscoelastic solid layer can be expressed in terms of $\tilde{u}_i(z)$ in a similar manner to give

$$\mathrm{d}_z\tilde{u}_z + \mathrm{i}k\tilde{u}_x = 0, \tag{48}$$

$$-\mathrm{i}k\tilde{p}_\mathrm{g} + \left(\frac{1}{\Gamma} - \mathrm{i}kc\eta_\mathrm{r}\right)(\mathrm{d}_z^2 - k^2)\tilde{u}_x = -Re\,k^2c^2\tilde{u}_x, \tag{49}$$

$$-\mathrm{d}_z\tilde{p}_\mathrm{g} + \left(\frac{1}{\Gamma} - \mathrm{i}kc\eta_\mathrm{r}\right)(\mathrm{d}_z^2 - k^2)\tilde{u}_z = -Re\,k^2c^2\tilde{u}_z. \tag{50}$$

These equations can be reduced to a single fourth-order differential equation for $\tilde{u}_z$:

$$(1 - \mathrm{i}kc\eta_\mathrm{r}\Gamma)(\mathrm{d}_z^2 - k^2)^2\tilde{u}_z + Re\,k^2c^2\Gamma(\mathrm{d}_z^2 - k^2)\tilde{u}_z = 0. \tag{51}$$

The linearized boundary conditions at the unperturbed interface position $z = 0$ between FENE-P fluid B and the solid layer are given by [14,28]:

$$\tilde{v}_z^\mathrm{b} = (-\mathrm{i}kc)\tilde{u}_z, \tag{52}$$

$$\tilde{v}_x^\mathrm{b} + [\mathrm{d}_z\bar{v}_x^\mathrm{b}]_{z=0}\tilde{u}_z = (-\mathrm{i}kc)\tilde{u}_x, \tag{53}$$

$$-\tilde{p}^\mathrm{b} + \tilde{\tau}_{zz}^\mathrm{b} = -\tilde{p}_\mathrm{g} + 2\left(\frac{1}{\Gamma} - \mathrm{i}kc\eta_\mathrm{r}\right)\mathrm{d}_z\tilde{u}_z, \tag{54}$$

$$\tilde{\tau}_{xz}^\mathrm{b} - \mathrm{i}k\bar{\tau}_{xx}^\mathrm{b}\tilde{u}_z = \left(\frac{1}{\Gamma} - \mathrm{i}kc\eta_\mathrm{r}\right)(\mathrm{d}_z\tilde{u}_x + \mathrm{i}k\tilde{u}_z). \tag{55}$$

Here, the second term in the left side of Eqs. (53) and (55) represent nontrivial contributions that arise as a result of the Taylor expansion of the mean flow quantities about the unperturbed fluid–solid interface. The boundary conditions for the displacement field at $z = -H$ are

$$\tilde{u}_z = 0, \qquad \tilde{u}_x = 0. \tag{56}$$

2.3.3. Neo-Hookean solid

The governing equations of the neo-Hookean solid are similarly linearized about the base state (see [24] for more details), and we obtain the following linearized stability equations in the limit of zero inertia in the solid:

$$\mathrm{d}_Z\tilde{w}_Z + \mathrm{i}k\tilde{w}_X - C_1\mathrm{i}k\tilde{w}_Z = 0 \tag{57}$$

$$-\mathrm{i}k\tilde{p}_\mathrm{g} + \frac{1}{\Gamma}(\mathrm{d}_Z^2 - k^2)\tilde{w}_X = 0, \tag{58}$$

$$\mathrm{i}kC_1\tilde{p}_\mathrm{g} + \frac{1}{\Gamma}(\mathrm{d}_Z^2 - k^2)\tilde{w}_Z - \mathrm{d}_Z\tilde{p}_\mathrm{g} = 0, \tag{59}$$

where $C_1 \equiv \mathrm{d}_z\bar{w}_x = (\Gamma/\bar{f}^\mathrm{b})\,\mathrm{d}_z\bar{v}_x^\mathrm{b}$ is the deformation gradient at base state in the neo-Hookean solid. As first pointed out by Gkanis and Kumar [24], these linearized equations show that the

term involving C_1 represents additional coupling (when compared with the linear viscoelastic solid model) between the base state deformation gradient and the horizontal gradients in the vertical displacement (Eq. (57)) and another additional coupling between the base state deformation gradient and pressure perturbation in the solid (Eq. 59). These additional couplings arise due to the nonlinearity of the governing equations in a neo-Hookean solid. These equations can be reduced to a single fourth-order differential equation for $\tilde{w}_Z$:

$$(\mathrm{i}kC_1 - \mathrm{d}_Z)(d_Z^2 - k^2)\left(C_1 + \frac{\mathrm{i}}{k}\mathrm{d}_Z\right)\tilde{w}_Z + \mathrm{i}k(\mathrm{d}_Z^2 - k^2)\tilde{w}_Z = 0. \tag{60}$$

The linearized interface conditions at the unperturbed fluid B – deformable solid interface $z = 0$ are obtained for the neo-Hookean model as

$$\tilde{v}_z^{\mathrm{b}} = -\mathrm{i}kc\tilde{w}_Z, \tag{61}$$

$$\tilde{v}_x^{\mathrm{b}} + [\mathrm{d}_z\tilde{v}_x^{\mathrm{b}}]_{z=0}\tilde{w}_Z = (-\mathrm{i}kc)\tilde{w}_X, \tag{62}$$

$$\tilde{\tau}_{xz}^{\mathrm{b}} - \mathrm{i}k\tilde{\tau}_{xx}^{\mathrm{b}}\tilde{w}_Z = \frac{1}{\Gamma}[\mathrm{d}_Z\tilde{w}_X + (C_1\mathrm{d}_Z + \mathrm{i}k(1 - C_1^2))\tilde{w}_Z], \tag{63}$$

$$-\tilde{p}^{\mathrm{b}} + \tilde{\tau}_{zz}^{\mathrm{b}} = -\tilde{p}_{\mathrm{g}} + \frac{2}{\Gamma}\mathrm{d}_Z\tilde{w}_Z. \tag{64}$$

Differential equations (31)–(33) for the two fluids and (48)–(50) for the solid layer along with interface and boundary conditions (Eqs. (52)–(56) for the linear viscoelastic solid, and Eqs. (61)–(64) for the neo-Hookean solid) completely specify the stability problem for the three-layer configuration of interest in this study. The complex wavespeed c is a function of W_α, μ_{r}, Γ, k, H, β, Σ, η_{r}, b^α, and Re.

3. Numerical method

For arbitrary values of k and μ_{r} and Re, there are no closed form solutions to the governing FENE-P stability equations, and so a numerical method must be used to solve the stability problem in general, which is described briefly here. A numerical integrator [29] combined with a Newton–Raphson iteration scheme are respectively used to solve the fourth-order ordinary differential equations in each layer and to solve for the eigenvalue. It is well known (see, for example, [30]) that this method is not guaranteed to capture all the eigenvalues of the problem, as this requires a good initial guess to converge to the desired solution. Consequently, a spectral method is often used to compute the eigenvalues of the stability problem in viscoelastic fluids (see, for example, the recent work of Arora and Khomami [27]). However, in this study, our primary interest is in tracking the two-fluid interfacial mode for FENE-P fluids, which becomes unstable in a rigid channel due to elasticity and viscosity stratification, and how this mode is affected by the deformable solid layer. This interfacial mode is accessible by a low-wavenumber asymptotic analysis for UCM fluids, and we numerically continue the UCM low-wavenumber results to FENE-P fluids for arbitrary wavenumbers by using the numerical procedure described below. In other words, since our interest is mainly in the understanding of the suppression or enhancement of the two-fluid interfacial mode, the shooting method suffices for the present purposes.

A fourth-order Runge–Kutta integrator with adaptive step size control is used to obtain numerical representations of the linearly independent solutions to the fourth-order differential equations. For fluid A, there are two linearly independent solutions consistent with the two boundary conditions at $z = 1$, and these are obtained by numerically integrating the fourth-order stability equation from $z = 1$ to $z = \beta$. The velocity field $\tilde{v}_z^{\mathrm{a}}$ in fluid A is then obtained as a linear combination of these two linearly independent solutions. For fluid B, which is bounded by fluid A and the solid layer on either side, we obtain four linearly independent solutions by numerically integrating from $z = \beta$ to $z = 0$. For the solid layer, we obtain two linearly independent solutions consistent with the boundary conditions at $z = -H$ by numerically integrating from $z = -H$ to $z = 0$. Thus, there are eight coefficients multiplying the linearly independent solutions (two in fluid A, four in fluid B, and two in the solid layer) in the three layers. The numerical solutions obtained in this manner are substituted in the eight interface conditions at $z = 0$ and $z = \beta$ (Eqs. (42)–(55)) and a 8×8 characteristic matrix is obtained. The determinant of the characteristic matrix is set to zero to obtain the characteristic equation, which is solved using a Newton–Raphson iteration scheme to obtain the complex wavespeed. It is well recognized that this shooting procedure needs a good initial guess in order to converge to the desired eigenvalue (the two-fluid interfacial mode in the present work). We take the initial guess from the previous study by Shankar [15], where a low-k asymptotic analysis was carried out for two-layer flow of UCM fluids past a linear viscoelastic solid. That asymptotic analysis yields an analytical expression for the wavespeed of the two-fluid interfacial mode, as a perturbation series in k for the case of two-layer flow of UCM fluids past a linear viscoelastic solid. In this study, we use the previous analytical expression as a starting point in the limit $b \gg 1$ and $k \ll 1$, and numerically continue those results to the case of FENE-P fluids $b \sim \mathrm{O}(100)$ and for finite values of k.

We have validated our numerical procedure and computer code by comparing our results for the special case of a single FENE-P Couette flow in a rigid channel with the recent results of Arora and Khomami [27], who have reported numerical results obtained using a spectral method. We compared the results from our numerical procedure for the special case of $\Gamma = 0$, $\mu_{\mathrm{r}} = 1$, $b^{\mathrm{a}} = b^{\mathrm{b}}$, and $W_{\mathrm{a}} = W_{\mathrm{b}}$ and for arbitrary values of the fluid thickness parameter β (i.e. $0 \le \beta \le 1$). In this special limiting case, our two-layer configuration reduces to that of a single layer plane Couette flow of an FENE-P fluid in a rigid channel. It must be noted that Arora and Khomami report eigenvalues for FENE-P fluid in the presence of solvent viscosity, and our numerical code is developed in general to account for solvent contribution as well. Under these conditions, our numerical code was able to successfully capture the Gorodtsov–Leonov modes in an FENE-P fluid reported in Figs. 1 and 2 of Arora and Khomami [27]. In addition, in the limit of $b \gg 1$ and $k \ll 1$, our numerical procedure was able to reproduce the low-wavenumber asymptotic results for two-layer UCM plane Couette flow past a linear

viscoelastic solid [15]. For the neo-Hookean solid case, our results were validated with the results reported in Shankar [14] and Gkanis and Kumar [24] under appropriate conditions.

4. Results

We now present the results obtained from the numerical method outlined above for the interfacial mode in two-layer plane Couette flow of viscoelastic fluids. The discussion of the results will be divided into three parts: first, we demonstrate how finite extensibility of the polymer chain affects the neutral stability diagrams significantly in the case of two-layer flow of FENE-P fluids in a rigid channel; secondly, we turn to the results obtained for the case of FENE-P flow past a linear viscoelastic solid, in order to examine how the finite extensibility of the polymer chain affects the predictions using the UCM model reported in the earlier study [15]; finally, we discuss the predictions obtained using the neo-Hookean solid model, and examine whether the use of the neo-Hookean model results in significant deviations when compared to the linear elastic solid model vis-á-vis the two-fluid interfacial mode. Before proceeding to discuss the results, it is pertinent here to point out that for the case of two-layer flow of viscoelastic fluids past a deformable solid layer, in addition to the two-fluid interfacial mode, there is also the possibility of the fluid–solid interface becoming unstable [15,28]. This is a finite-wavenumber instability which occurs when the nondimensional parameter Γ exceeds a critical value for a fixed Weissenberg number. In the earlier study of two-layer UCM flow past a deformable solid layer [15], it was found that the critical Γ required for this instability is typically three to four orders of magnitude higher than the values of Γ required for suppression or enhancement of the two-fluid interfacial mode. A similar conclusion is arrived in this study for FENE-P fluids a little later (see Fig. 17). For this reason, we focus our efforts here mainly on the two-fluid interfacial mode and study the effect of solid deformability on this mode.

4.1. Two-layer flow of FENE-P fluids in a rigid channel

It is first useful to recall that for two-layer Couette flow of UCM fluids with equal viscosities, Chen [2] showed using a long-wave asymptotic analysis that the two-fluid interfacial mode is unstable when the more elastic fluid is of smaller thickness. In terms of the nomenclature of the present study, this translates to: for $\mu_r = 1$, instability occurs when $\beta < 1/2$, $W_b > W_a$, and $\beta > 1/2$, $W_a > W_b$; the two-layer system is stable otherwise according to the UCM model. For the special case of $\mu_r = 1$ and $\beta = 1/2$, the UCM results show that the system is neutrally stable for arbitrary values of W_a and W_b. We first examine the effect of finite extensibility parameter b on this result for two-layer Couette flow of FENE-P fluids. In all the results that follow, we set the finite extensibility parameter $b = 100$ for both the FENE-P fluids. For the rest of this discussion of two-layer FENE-P flow in a rigid channel, we further set $k = 0.01$ in order to stay in the long-wave limit, and $Re = 1$ without loss of generality. We have verified that the results obtained for $Re = 1$ are quite close to the creeping-flow limit of $Re = 0$.

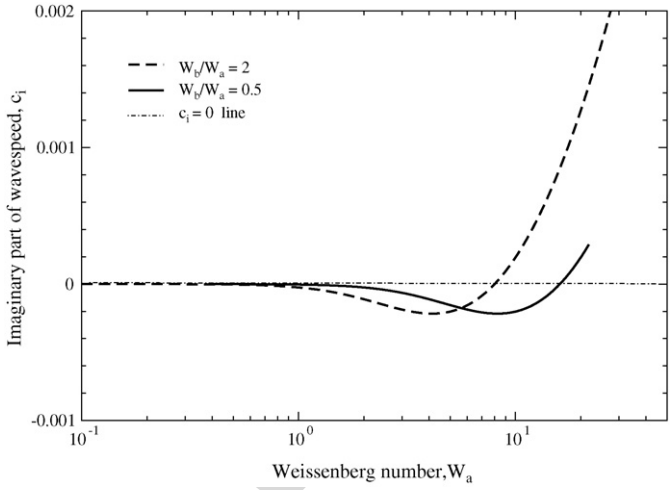

Fig. 2. Effect of increase in W_a on the stability of the two-fluid interfacial mode for FENE-P fluids in a rigid channel: $\beta = 0.5$, $\mu_r = 1$, $Re = 1$, $\Sigma = 0$, and $k = 0.01$, for two different values of W_b/W_a. For these parameters, the two-layer UCM Couette flow is always stable.

In general, we expect the two-layer FENE-P results to approach the two-layer UCM results for small values of W_a and W_b. The implications of finite extensibility such as shear-rate dependence of viscosity and first normal stress difference will start affecting the stability only at finite values of W_a and W_b. We first consider the case of $\beta = 1/2$ and the ratio of zero-shear viscosities $\mu_r = 1$. In Fig. 2 we examine the effect of increasing W_a on c_i (the imaginary part of wavespeed, proportional to the growth rate) for two fixed values of W_b/W_a. Our results show that upon increase of W_a, the two-fluid mode in FENE-P fluids does become unstable after a critical value of W_a, and this critical value is smaller for larger values of W_b/W_a. This shows that even in the simplest configuration of equal fluid thickness and with identical zero shear viscosities, the shear-rate dependence of the viscosity and normal stress difference qualitatively alters the stability behaviour in FENE-P fluids as W_a and W_b are increased. This result can be understood by noting that in the FENE-P case, it is only the zero-shear viscosities that are equal in both the fluids; since W_a and W_b are different, at finite Weissenberg numbers, the actual (i.e. shear-rate dependent) viscosities will be different. The earlier asymptotic analysis [15] for UCM two-layer flow shows that for unequal viscosities in the two fluids, even if $\beta = 1/2$ the flow is unstable at appropriate values of Weissenberg number. The two-layer result for FENE-P fluids with equal zero-shear viscosities but different Weissenberg numbers can thus be understood in light of this UCM result for unequal viscosities.

Fig. 3 shows the neutral stability curve (continuous line in the figure) demarcating stable and unstable zones for $\beta = 1/2$ and $\mu_r = 1$ in the W_a versus $W_b/W_a = (\lambda_b/\lambda_a)$ plane. This shows that the critical value of W_a required for destabilizing the two-fluid interface decreases with increase in W_b/W_a. Another feature to be noted in this figure is the presence of an 'isolated neutral line' when $W_b/W_a = 1$. For $\beta = 1/2$ and for $\mu_r = 1$, when $W_b = W_a$, the two layers become identical in all respects and reduce to the limit of a single layer. In this limit, the two-fluid interfacial mode reduces into an isolated neutral mode which nei-

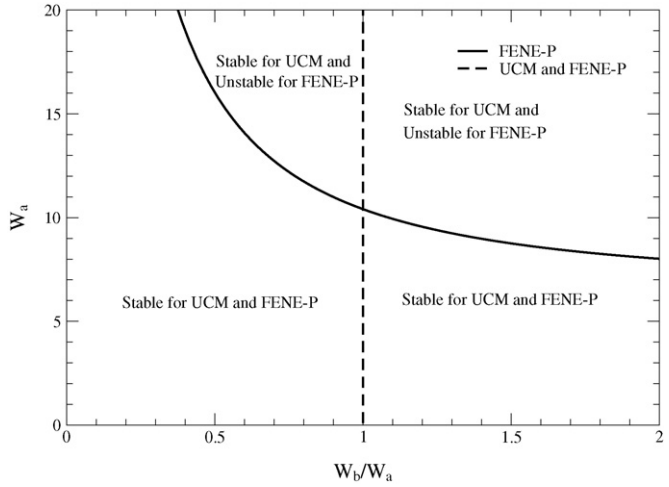

Fig. 3. Neutral stability diagram in the W_a vs. $W_b/W_a = \lambda_b/\lambda_a$ plane for two-layer FENE-P flow in a rigid channel with $\beta = 0.5$ and $\mu_r = 1$, $Re = 1$, $\Sigma = 0$, and $k = 0.01$. The continuous line shows the transition between stable and unstable modes in the FENE-P case, and the broken line is an 'isolated neutral line' where the growth rate becomes zero, but there is no transition between stable and unstable modes. The two-layer UCM case is always stable.

ther grows nor decays. Whether one is in the stable or unstable zone of the stability boundary in Fig. 3, the growth rate (i.e. c_i) will become zero at $W_b/W_a = 1$. Thus, the isolated neutral line does not signify a transition from stable to unstable modes (or vice versa), but merely shows that c_i will become zero in that line.

Fig. 4 shows the effect of decreasing the thickness parameter β to 0.4, but with equal zero-shear viscosities $\mu_r = 1$. Here, for the UCM case, when one plots W_a versus W_b/W_a, the region to the left of the neutral stability curve (a vertical line at $W_b/W_a = 1$) is stable, and the region to the right of the neutral curve is unstable (i.e. more elastic fluid occupying smaller thickness). However, for the case of FENE-P fluids, the stability boundaries are significantly different: there is a zone of instability for the FENE-P case when it is stable for the UCM case, and there is a region of stability in the FENE-P case when it is unstable

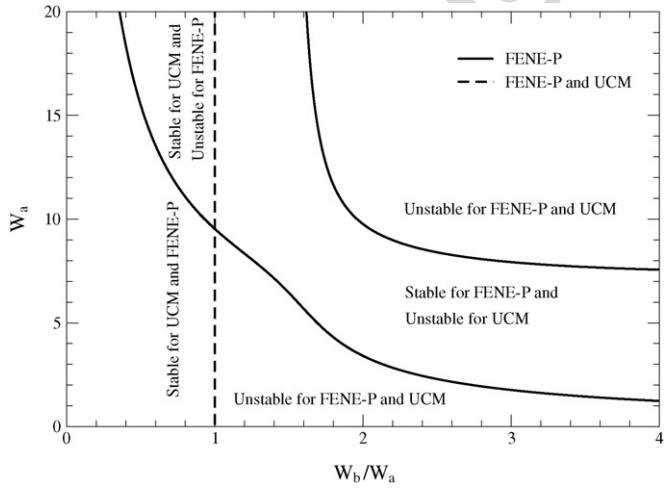

Fig. 4. Neutral stability diagram for two-layer FENE-P flow in a rigid channel in the W_a–(W_b/W_a) plane for $\mu_r = 1$, $\beta = 0.4$, $Re = 1$, $\Sigma = 0$, $k = 0.01$. The continuous line indicates the transition from stable to unstable modes (and vice versa) for FENE-P fluid, and the dotted line indicates the transition for both FENE-P and UCM fluids.

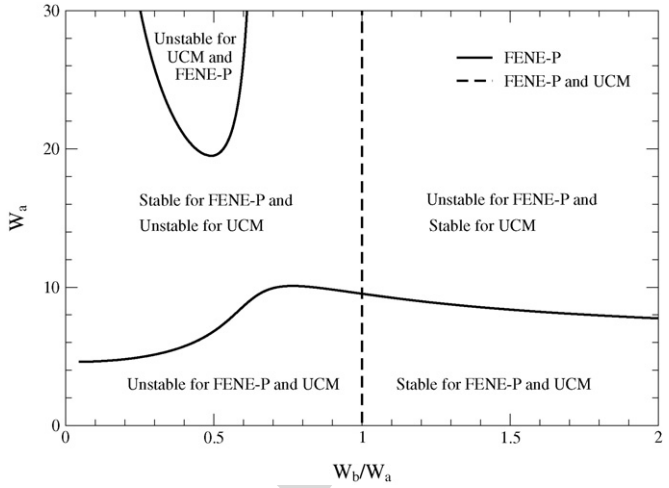

Fig. 5. Neutral stability diagram for two-layer FENE-P flow in a rigid channel in the W_a–(W_b/W_a) plane for $\mu_r = 1$, $\beta = 0.6$, $Re = 1$, $\Sigma = 0$, $k = 0.01$. The continuous line indicates the transition from stable to unstable modes (and vice versa) for FENE-P fluid, and the dotted line indicates the transition for both FENE-P and UCM fluids.

in the UCM case. Here, the dotted line with $W_b/W_a = 1$ is a neutral line for both FENE-P and UCM fluids, and unlike the $\beta = 1/2$ case discussed above, it indeed represents a crossover from stable to unstable modes. As mentioned before, all these results are in the low-wavenumber limit, with $k = 0.01$ set in the numerical study. For $\beta = 0.4$ and $W_b/W_a > 1$, the UCM case is unstable, while in a band of W_a the FENE-P case is stable as shown in Fig. 4. It is of interest to ask if this stable behaviour of the FENE-P fluids is only in the low-k limit or whether this extends to finite values of k. We chose a point $W_a = 8$ and $W_b = 16$ and computed the c_i versus k curve for the two-layer FENE-P case. c_i values are always negative, thus indicating that the stability of the two-fluid mode at low values of k indeed continues to finite wavenumbers in the FENE-P fluid.

Fig. 5 shows the neutral stability diagram for $\beta = 0.6$ and $\mu_r = 1$. For the UCM case, the system is unstable when

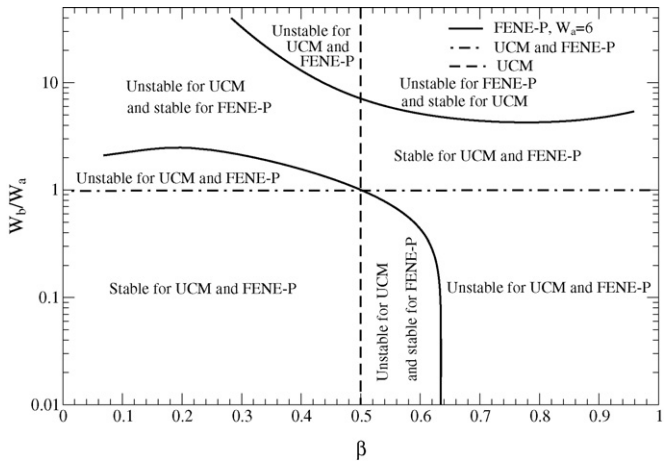

Fig. 6. Neutral stability diagram for two-layer FENE-P flow in a rigid channel in the (W_b/W_a)–β plane for $\mu_r = 1$, $W_a = 6$, $Re = 1$, $k = 0.01$. The continuous line indicates the transition from stable to unstable modes for FENE-P fluid, the dash-dotted line indicates the transition for both FENE-P and UCM fluids, and the dashed line indicates the transition only for UCM fluids.

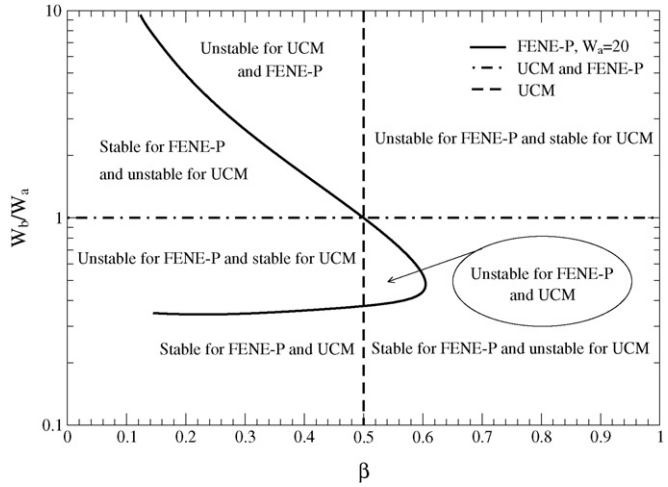

Fig. 7. Neutral stability diagram for two-layer FENE-P flow in a rigid channel in the (W_b/W_a)–β plane for $\mu_r = 1$, $W_a = 20$, $Re = 1$, $k = 0.01$. The continuous line indicates the transition from stable to unstable modes for FENE-P fluid, the dash-dotted line indicates the transition for both FENE-P and UCM fluids, and the dashed line indicates the transition only for UCM fluids.

$W_b/W_a < 1$ and is stable when $W_b/W_a > 1$. For this case too, as for $\beta = 0.4$, the FENE-P fluids have significantly different stability boundaries compared to the UCM case, with new stable and unstable regions appearing for FENE-P fluids in the W_a–(W_b/W_a) plane. Figs. 3–5, respectively, for $\beta = 0.5$, 0.4 and 0.6 further illustrate how the stability boundaries change qualitatively for small changes in the thickness parameter β for FENE-P fluids.

In Fig. 6, we show the stability boundaries in the (W_b/W_a)–β plane for $\mu_r = 1$. For the simple case of two-layer UCM flow without any viscosity contrast (i.e. $\mu_r = 1$), the stable and unstable regions separate into four quadrants as shown in Fig. 6. For UCM fluids, the stable and unstable quadrants are independent of the individual values of W_a or W_b. However, for two-layer FENE-P flow, as shown in Figs. 6 and 7, the

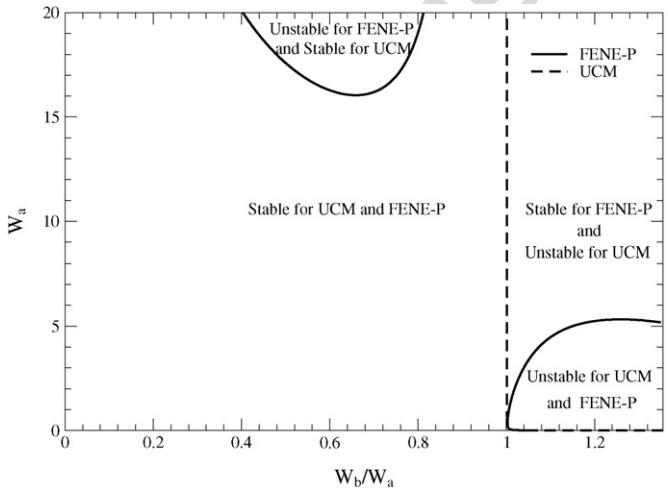

Fig. 8. Effect of variation in the ratio of zero-shear viscosities μ_r on the neutral stability diagram for two-layer FENE-P flow in a rigid channel in the W_a–(W_b/W_a) plane for $\mu_r = 1.05$, $\beta = 0.4$, $Re = 1$, $k = 0.01$. The continuous line indicates the transition from stable to unstable modes for FENE-P fluid, and the dotted line indicates the transition for UCM fluids.

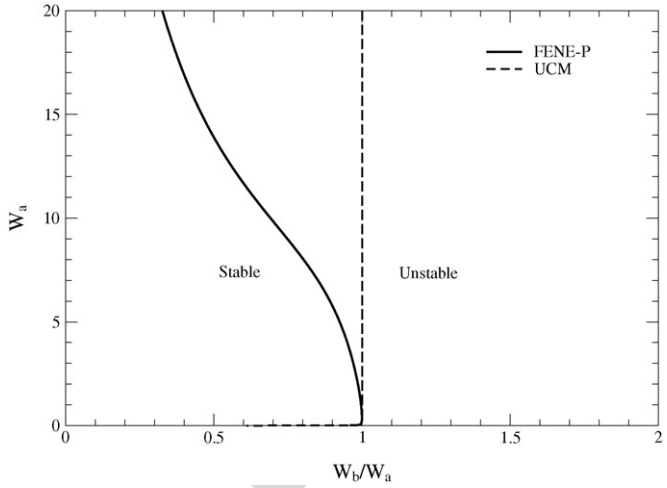

Fig. 9. Effect of variation in the ratio of zero-shear viscosities μ_r on the neutral stability diagram for two-layer FENE-P flow in a rigid channel in the W_a–(W_b/W_a) plane for $\mu_r = 0.95$, $\beta = 0.4$, $Re = 1$, $k = 0.01$. The continuous line indicates the transition from stable to unstable modes for FENE-P fluid, and the dotted line indicates the transition for UCM fluids.

stable and unstable regions in the (λ_b/λ_a)–β plane are actually a function of W_a, thus showing how the shear-rate (i.e. W_a) dependence of the viscosity and normal stress difference affects the neutral stability boundaries.

We next examine the effect of changing the ratio of zero-shear viscosities μ_r on the neutral stability diagram. Figs. 8 and 9 demonstrate how drastically the stability boundaries change for FENE-P fluids as μ_r is changed to 1.05 and 0.95, respectively, when compared to the $\mu_r = 1$ case shown in Fig. 4. In marked contrast, the UCM stability boundary is virtually unaffected by such small changes in μ_r. Further decrease of μ_r to 0.5 showed that the neutral curve is qualitatively similar to $\mu_r = 0.95$ but zone of instability of the FENE-P case is extended further compared to the UCM case. Fig. 10 shows the change in stability boundaries as μ_r is increased to 4. Here again, the FENE-P fluid has a larger zone of instability compared to the UCM fluid. By

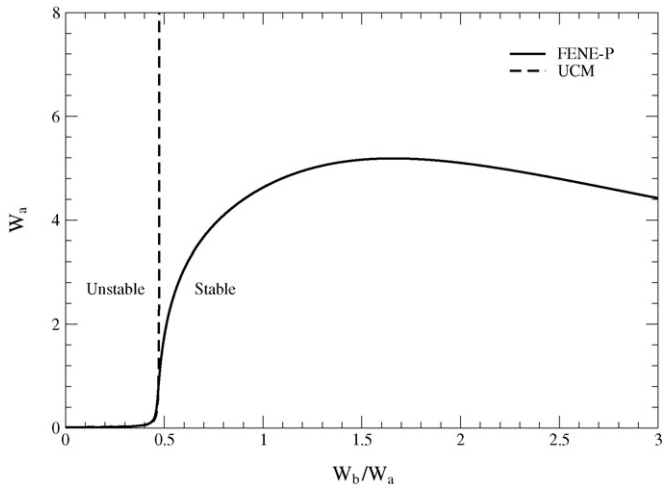

Fig. 10. Neutral stability diagram for two-layer FENE-P flow in a rigid channel in the W_a–(W_b/W_a) plane for $\mu_r = 4.0$, $\beta = 0.4$, $Re = 1$, $k = 0.01$. The continuous line indicates the transition from stable to unstable modes for FENE-P fluid, and the dotted line indicates the transition for UCM fluid.

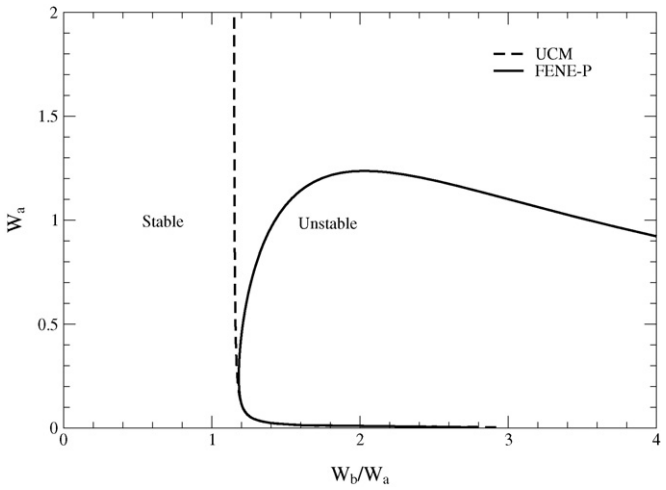

Fig. 11. Neutral stability diagram for two-layer FENE-P flow in a rigid channel in the W_a–(W_b/W_a) plane for $\mu_r = 2.0$, $\beta = 0.2$, $Re = 1$, $k = 0.01$. The continuous line indicates the transition from stable to unstable modes for FENE-P fluid, and the dotted line indicates the transition for UCM fluid. This figure shows that the FENE-P case is stable in a larger parametric zone than the UCM fluid.

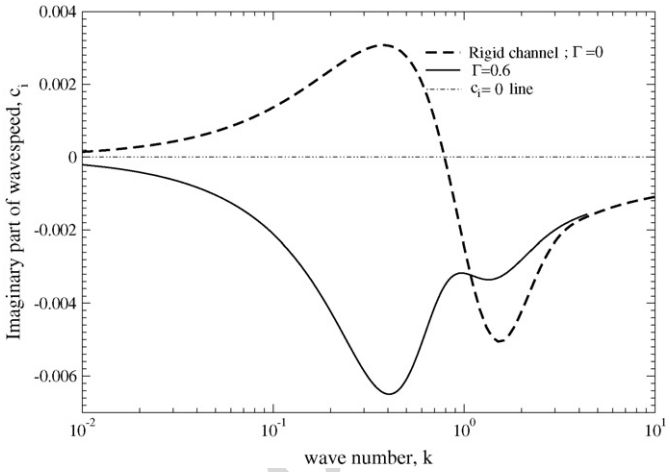

Fig. 12. Effect of solid layer deformability on the two-fluid interfacial mode in FENE-P fluids: variation of imaginary part of wavespeed c_i with wavenumber k. Data for $\mu_r = 0.8$, $\beta = 0.4$, $W_a = 6$, $W_b = 5.4$, $Re = 1$, $\Sigma = 0.2$, $H = 1$, $\eta_r = 0.1$.

contrast, for $\mu_r = 2$ and $\beta = 0.2$ (Fig. 11), the FENE-P fluid is stable in a larger parametric range when compared to the UCM fluid. For $\mu_r \neq 1$, this is one of the very few instances when the two-layer FENE-P flow is more stable compared to the two-layer UCM flow. In general, however, the opposite is found to be the case.

Before proceeding to discuss the effect of the deformable solid layer, it is useful to summarize the key conclusions from our results for two-layer Couette flow of FENE-P fluids in a rigid channel. Our numerical results demonstrate that the stability boundaries are significantly altered in the FENE-P case when compared to the UCM case, and that the stability boundaries are a sensitive function of the viscosity ratio μ_r. To the best of our knowledge, we are not aware of prior work in this area presenting such detailed numerical results for two-layer flow of FENE-P fluids. In the previous work by Ganpule and Khomami [11], a modified Phan–Thien–Tanner (MPTT) model was used to study the two-layer pressure-driven plane Poiseuille flow in a rigid channel, and two sets of neutral curves were presented in the (W_b/W_a)–β plane. However, the data presented were for $W_a = 0.1$, which is on the lower side in order to observe any significant departure from the UCM results, and this was indeed the case in their results.

While our motivation for computing these neutral stability curves is to examine the effect of a deformable solid layer coating on the two-layer instability, the above results for two-layer FENE-P flow in rigid channels could as such be of utility, especially in the comparison of experimental observations with theoretical predictions of two-layer interfacial instability in polymeric liquids.

4.2. Results from the linear viscoelastic solid model

We now turn to examine the effect of a soft deformable solid layer coating on the two-layer instability in FENE-P fluids. In this section, we discuss the results obtained using a linear viscoelastic model for the solid layer. The earlier work of Shankar [15] has carried out a study for two-layer UCM plane Couette flow past a linear viscoelastic solid, and it was shown using both low wavenumber asymptotic analysis and numerical computations that the two-layer instability could be completely suppressed or triggered by the deformable solid layer. In the present discussion for two-layer plane Couette flow of FENE-P fluids, we wish to address the following questions:

- Will the stabilizing nature of the solid layer on the two-layer instability predicted for UCM fluids remain so in two-layer FENE-P flow?
- What will be the consequence of using the FENE-P model on the shear modulus of deformable solid the required for suppression of the instability?
- The two-layer FENE-P flow was shown to have a larger zone of instability compared to two-layer UCM flow; will the solid layer still have a stabilizing effect for these 'new' unstable regions present only for FENE-P fluids?

The numerical results for FENE-P fluid are obtained by using the low-wavenumber asymptotic results [15] as a starting point, and by numerically continuing the extensibility parameter b from very large values (UCM fluid) to $b = 100$ (FENE-P fluid). Fig. 12 shows the variation of c_i with k for the two-fluid interfacial mode with specified values of $W_a = 6$, $W_b = 5.4$, $\mu_r = 0.8$, $\beta = 0.4$, $Re = 1$, $\Sigma = 0.2$, $H = 1$, $\eta_r = 0.1$. The limit of a rigid channel is obtained by setting $\Gamma = 0$ (elastic stresses in the solid layer very large compared to viscous stresses in the two fluids), and the figure shows (dashed line) that the two-layer interfacial mode is unstable from $k \ll 1$ to $k \sim O(1)$. In our ensuing discussion, we have used nominal values of the interfacial tension parameter Σ between the two fluids, and for viscosity ratio η_r between the fluid B and the linear viscoelastic solid layer. The continuous line in Fig. 12 shows the effect of increase in solid layer deformability parameter Γ from zero (rigid wall) to

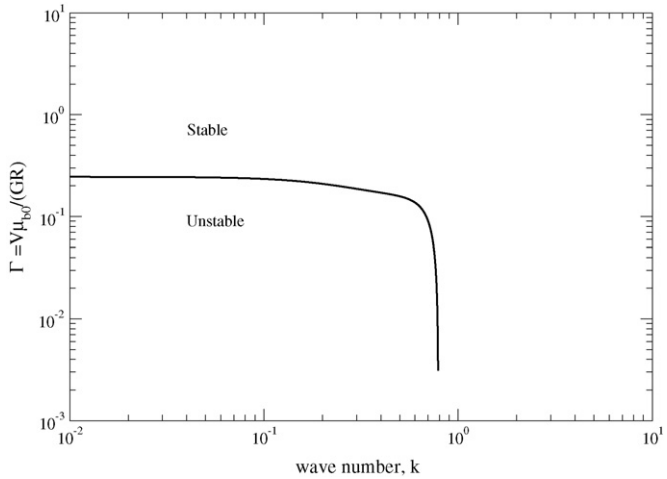

Fig. 13. Neutral stability curve in the Γ–k plane for the FENE-P two-fluid interfacial mode in the presence of the deformable solid layer showing suppression of interfacial instability at all wavenumbers. Data for $\mu_r = 0.8$, $\beta = 0.4$, $W_a = 6$, $W_b = 5.4$, $Re = 1$, $\Sigma = 0.2$, $H = 1$, $\eta_r = 0.1$.

0.6, and the interfacial instability is completely suppressed at all wavenumbers. At higher wavenumbers ($k > 5$), it is seen that the two curves corresponding to rigid solid layer and soft solid layer coincide with each other, indicating that for these short wavelength fluctuations, the disturbance velocities are more confined near the two-fluid interface and the deformability of the solid layer has no effect on such short wavelength fluctuations. It is useful to present the results in terms of a neutral stability diagram in the Γ–k plane where the stable and unstable regions will be demarcated; such a plot for the above set of parameters is shown in Fig. 13. For $\Gamma \to 0$, the deformable solid layer approaches the rigid limit, and so one expects the two-layer instability to be present. As Γ is increased beyond a critical value as given by the neutral curve, the two-layer instability is suppressed at all wavenumbers. A similar prediction for a different set of parameters for the FENE-P fluids is shown in Fig. 14. We have verified for a wide range of parameters that when the two-layer mode is

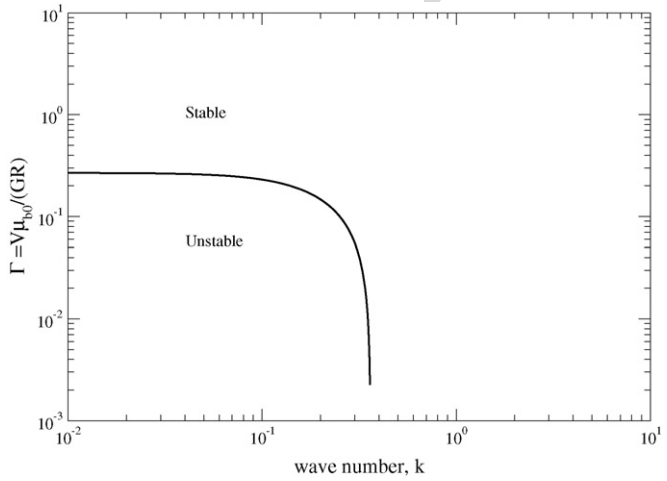

Fig. 14. Neutral stability curve in the Γ–k plane for the FENE-P two-fluid interfacial mode in the presence of the deformable solid layer showing suppression of interfacial instability at all wavenumbers. Data for $\mu_r = 0.2$, $\beta = 0.4$, $W_a = 6$, $W_b = 4.8$, $Re = 1$, $\Sigma = 0$, $H = 1$, $\eta_r = 0.5$.

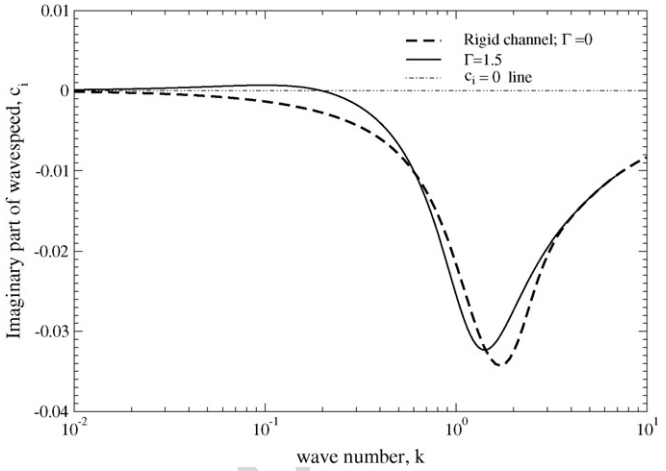

Fig. 15. Destabilization of the two-fluid interfacial mode in FENE-P fluids by the deformable solid layer. Data for $\mu_r = 0.5$, $\beta = 0.8$, $W_a = 3$, $W_b = 2.4$, $Re = 1$, $\Sigma = 0.4$, $H = 0.6$, $\eta_r = 0.1$.

unstable in FENE-P fluids, the deformable solid layer tends to have a stabilizing effect on the instability leading to complete suppression at all wavenumbers. Thus, the central conclusion of the earlier analysis for two-layer UCM flow concerning the suppression of interfacial instability carries over to the more realistic FENE-P model as well. This is one of the main conclusions of the present study.

Fig. 15 shows the opposite effect, viz., destabilization of the two-fluid interface in FENE-P fluids by the deformable solid layer, when the interfacial mode is completely stable in flow past a rigid surface. Here again, the solid layer destabilizes the two-fluid mode for $k \to 0$ to $k \sim O(1)$, but the two curves corresponding to a rigid solid and deformable solid merge with each other for $k > 3$ for the same reason outlined above for short wavelength fluctuations. The neutral stability curve characterizing the parameter Γ required for destabilizing the two-fluid interface is shown in Fig. 16.

The discussion thus far has demonstrated that the deformable solid layer has a stabilizing effect when the two-fluid mode is un-

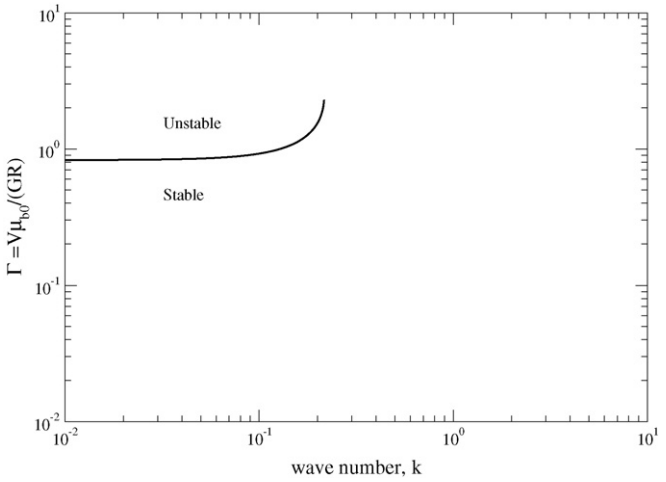

Fig. 16. Neutral stability curve in the Γ–k plane for the destabilization of FENE-P two-fluid interfacial mode by the deformable solid layer. Data for $\mu_r = 0.5$, $\beta = 0.8$, $W_a = 3$, $W_b = 2.4$, $Re = 1$, $\Sigma = 0.4$, $H = 0.6$, $\eta_r = 0.1$.

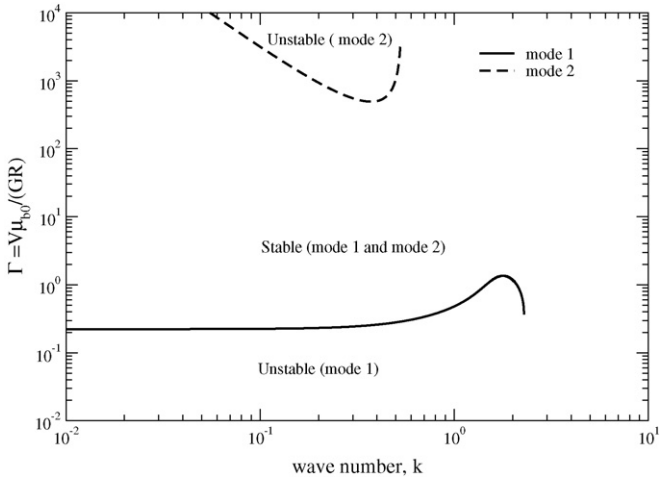

Fig. 17. Neutral stability curve in the Γ–k plane for both the two-fluid interfacial mode ("mode 1") and the fluid-solid mode ("mode 2") in FENE-P fluids. Result illustrating the wide gap between the two neutral curves. Data for $\mu_r = 0.5$, $\beta = 0.4$, $W_a = 1$, $W_b = 2$, $Re = 1$, $\Sigma = 0.25$, $H = 0.7$, $\eta_r = 0.6$.

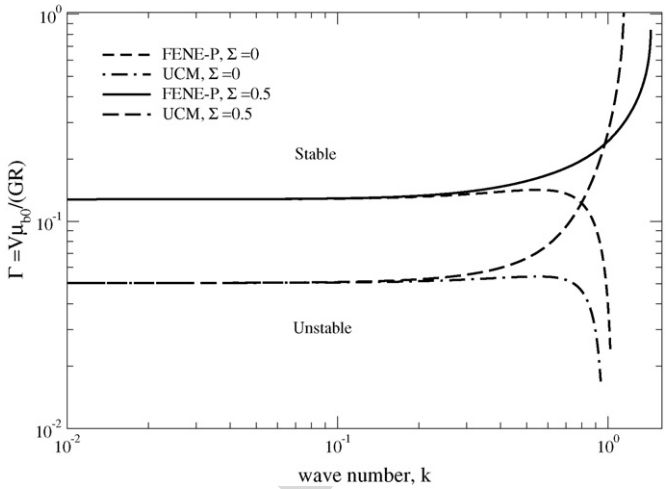

Fig. 18. Neutral stability curve in the Γ–k plane for the two-fluid interfacial mode obtained for both FENE-P and UCM fluids. Data for $\mu_r = 0.2$, $\beta = 0.4$, $W_a = 1.8$, $W_b = 4$, $Re = 1$, $H = 1$, $\eta_r = 0$.

stable, and it has a destabilizing effect when the two-fluid mode is stable in rigid channels. In the previous study of Shankar and Kumar [28], it was shown that the interface between an UCM fluid could also become unstable when the parameter Γ increases beyond a critical value. If two-layer viscoelastic flows are to be suppressed by soft solid layer coatings, it must be ensured that the fluid–solid interfacial instability is not readily excited due to the deformability of the solid. Using the result reported for the fluid–solid interfacial instability in the case of UCM two-layer flow [15] as a starting guess, we have numerically continued the neutral curve for the fluid B–solid interfacial instability to FENE-P fluids. The neutral stability curve for the fluid B–solid interfacial instability for FENE-P fluids is shown in Fig. 17, along with the neutral curve for the two-fluid interfacial mode. This result shows that there is a wide gap of Γ values in which both the modes are stable, and the two neutral curves are separated by Γ values varying by three to four orders of magnitude. Thus, it can be safely concluded that the suppression of the two-fluid interfacial mode by the deformable solid layer can be achieved without exciting the fluid B–solid interfacial mode.

In Fig. 18, we compare the neutral curves obtained for both UCM and FENE-P two-layer flows in the presence of the deformable solid layer. In this figure, we also illustrate the effect of nonzero interfacial tension of the two-fluid interface on the neutral curve, which suppresses any high-k instability of the two-layer flow. For the parameter values chosen, it was found that two-layer FENE-P flow in a rigid channel has larger growth rates than that for UCM flow. Consequently, one would expect the solid deformability parameter Γ required for suppressing the instability to be larger for the FENE-P model. This is indeed found to be the case in Fig. 18. In contrast to this behaviour, in Fig. 19, we find that the Γ required for suppressing the instability is smaller for FENE-P case compared to the UCM case, even though the two-fluid mode for FENE-P fluids has a larger growth rate compared to UCM fluids as shown in Fig. 20. This behaviour can be understood from the fact that the stabilizing contribution from the deformable solid layer is not just a function of Γ, but also the viscosity ratio of the two fluids, and thickness ratio. This was found to be the case in the earlier asymptotic analysis of UCM two-layer flow. Thus, although the destabilizing contribution from the two-fluid instability is larger for FENE-P fluids in Fig. 20, the stabilizing contribution from the deformable solid layer is also larger compared to UCM, thus resulting in a smaller Γ value required for suppressing the two-layer instability.

4.3. Results from the neo-Hookean solid model

We now turn to the comparison of the results obtained from the neo-Hookean solid model with that of linear elastic solid model. In a recent study, Gkanis and Kumar [26] have shown that for the case of flow down an inclined plane at zero Reynolds number, the results from neo-Hookean model differed qualitatively from that of linear elastic model. The linear elastic model is strictly valid when the base-state strain is small compared to 1. In the present problem the strain in the base-state in the

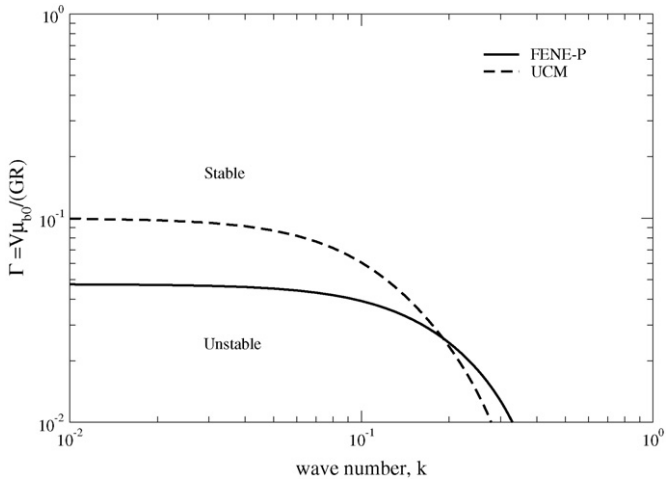

Fig. 19. Neutral stability curve showing that the Γ required for suppression of the two-fluid instability in FENE-P fluids is lower than that for UCM fluids, even though FENE-P is more unstable than UCM for this configuration. Data for $\mu_r = 4$, $\beta = 0.4$, $W_a = 2$, $W_b = 0.8$, $Re = 1$, $H = 1.315$, $\Sigma = 0.1$, $\eta_r = 0$.

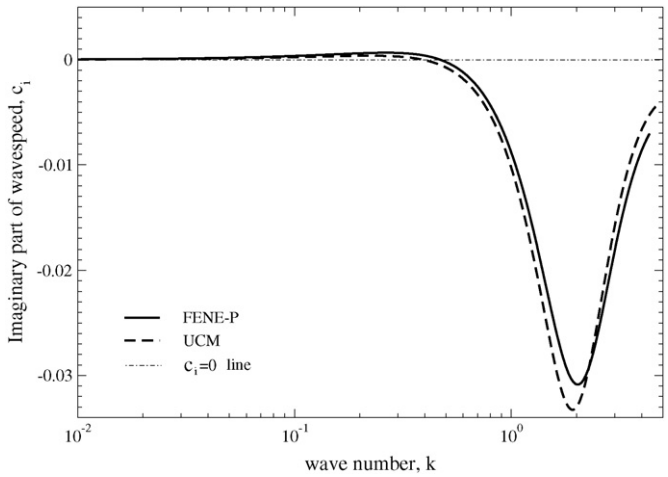

Fig. 20. c_i vs. k curve showing that the two-fluid mode in FENE-P fluids is more unstable in rigid channels than UCM fluids. Data for $\mu_r = 4$, $\beta = 0.4$, $W_a = 2$, $W_b = 0.8$, $Re = 1$, $\Sigma = 0$.

solid layer is proportional to Γ (Section 2.2), and in the results presented above, the numerical value of Γ required for instability suppression is indeed small compared to 1. Consequently, we might expect the linear elastic solid model to be accurate in so far as the prediction of the neutral curve for the two-fluid mode is concerned. In addition, it can be readily verified that the extra terms that appear in the linearized neo-Hookean solid equations and boundary conditions (see Section 2.3.3) do not make a contribution in the limit of small k, and the linearized neo-Hookean equations become identical to the stability equations for the linear elastic solid model as $k \ll 1$. Thus, at low k, the earlier asymptotic predictions for two-layer UCM flow past a linear elastic solid will remain valid even for the neo-Hookean case. Since the two-fluid interfacial instability is essentially a low-k instability, one might further expect the extra terms in the neo-Hookean equations not to affect the results significantly even at finite values of k. We verify this below by comparing the results obtained from the linear elastic model and the neo-Hookean model for the solid layer. Since Re does not play a very

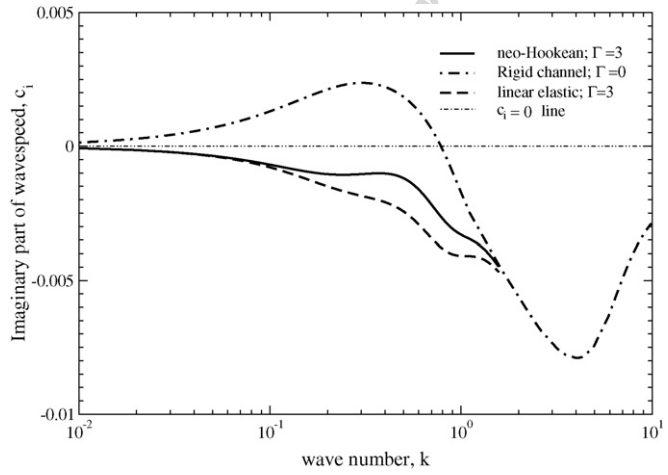

Fig. 21. Comparison of c_i vs. k curves for results obtained for stabilization of two-fluid mode in FENE-P fluids using both linear elastic and neo-Hookean solid models. Data for $\mu_r = 2$, $\beta = 0.8$, $W_a = 5$, $W_b = 6$, $Re = 0$, $H = 0.4$, $\Sigma = 0.1$.

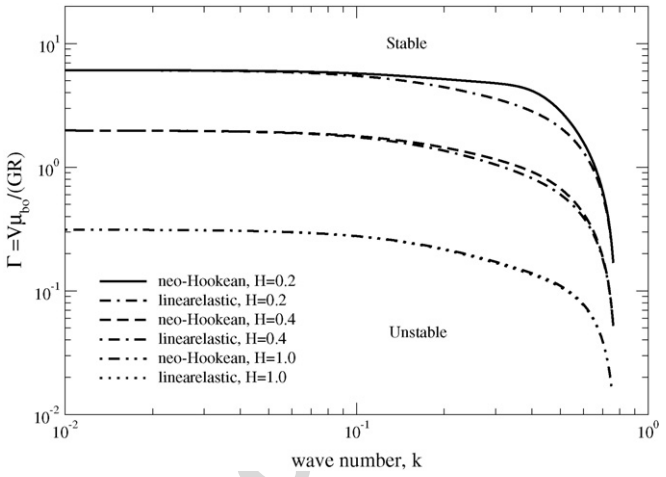

Fig. 22. Comparison of neutral stability curves for results obtained for suppression of two-fluid mode in FENE-P fluids using both linear elastic and neo-Hookean solid models. Data for $\mu_r = 2$, $\beta = 0.8$, $W_a = 5$, $W_b = 6$, $Re = 0$, $\Sigma = 0.1$.

significant role in the instability due to elasticity stratification, we have set $Re = 0$ in the following comparisons.

In Fig. 21, we show the c_i versus k curves for two-layer FENE-P flow past both linear elastic and neo-Hookean solids for a given set of parameters. This shows that the c_i versus k curves for both the models merge with each other for small values of k, and there is a small deviation at finite values of k. Importantly, however, both the linear elastic model and the neo-Hookean model both predict the suppression of the instability at all wavenumbers. In Fig. 22, we show the neutral stability curves in Γ–k plane for both linear elastic and neo-Hookean models, at three different values of solid thickness H. This comparison shows that as H increases from 0.2 to 1, the critical Γ required for suppression decreases, and agreement between the two solid models gets progressively better. At $H = 1$, the difference between the two curves is indistinguishable. We have verified that similar trend continues for a variety of other parameter regimes as well. Thus, our numerical results reveal that for the purposes of prediction of suppression of two-layer instability, the linear elastic solid model proves adequate.

5. Conclusions

A numerical study of the interfacial instability in two-layer plane Couette flow of FENE-P fluids past a deformable solid layer was carried out with the objective of extending the previous analysis [15] for UCM fluids to more realistic models for the viscoelastic fluids and the deformable solid. For two-layer plane Couette flow of FENE-P fluids past rigid surfaces, the present study provides new results for the neutral stability curves demarcating stable and unstable regions for the two-fluid interfacial instability driven by elasticity and viscosity stratification. Our results show that the stability boundaries are significantly altered for two-layer flow of FENE-P fluids when compared to those for UCM fluids. Also, the stability boundaries were sensitively dependent on the ratio of zero-shear viscosities of the two fluids. In general, we find the two-layer flow of FENE-P fluids

to be unstable in a larger range of parameters compared to the UCM model. This modification in the neutral stability curves is mainly a consequence of the shear-rate dependent first normal stress difference and shear-rate dependent viscosity, which alter the driving force for the interfacial instability. These results for two-layer plane Couette flow FENE-P fluids in rigid channels could be of utility in future comparisons of experimental observations involving polymeric liquids with theoretical predictions.

The effect of solid layer deformability on the interfacial instability in FENE-P fluids is studied in detail using both the linear viscoelastic and neo-Hookean models for the solid, and it is shown in general that when the two-fluid mode is unstable in rigid channels, the deformability of the solid layer could completely suppress the interfacial instability at all wavenumbers. Results were also presented wherein the solid layer has a destabilizing effect on the interfacial mode, when it is stable in flow past rigid surfaces. Another general trend that emerges is that the shear modulus required for suppressing the interfacial instability is generally smaller for FENE-P fluids when compared to UCM fluids, although there were few parameter ranges where the opposite is true. Results obtained using a linear elastic model for the deformable solid were compared with those obtained from a more rigorous neo-Hookean solid, and results from both models agreed very well for the two-fluid interfacial mode. In conclusion, the present study augments the earlier predictions [15] for two-layer flow of UCM fluids past a linear elastic solid, by extending them to more realistic FENE-P model for the fluids and neo-Hookean model for the solid. We have demonstrated that the main conclusion of suppression of interfacial instability by a deformable solid layer remains unaffected by the use of more accurate models for the fluid and the solid.

References

[1] Y. Renardy, Stability of the interface in two-layer Couette flow of upper convected Maxwell liquids, J. Non-Newtonian Fluid Mech. 28 (1988) 99–115.

[2] K. Chen, Elastic instability of the interface in Couette flow of two viscoelastic liquids, J. Non-Newtonian Fluid Mech. 40 (1991) 261–267.

[3] Y.-Y. Su, B. Khomami, Purely elastic interfacial instabilities in superposed flow of polymeric fluids, Rheol. Acta 31 (1992) 413–420.

[4] Y.-Y. Su, B. Khomami, Interfacial stability of multilayer viscoelastic fluids in slit and converging channel die geometries, J. Rheol. 36 (1992) 357–387.

[5] G.M. Wilson, B. Khomami, An experimental investigation of interfacial instabilities in the multilayer flow of viscoelastic fluids; Part I. Incompatible polymer systems, J. Non-Newtonian Fluid Mech. 41 (1992) 355.

[6] G.M. Wilson, B. Khomami, An experimental investigation of interfacial instabilities in the multilayer flow of viscoelastic fluids; Part II. Elastic and nonlinear effects in incompatible polymer systems, J. Rheol. 37 (1993) 315.

[7] G.M. Wilson, B. Khomami, An experimental investigation of interfacial instabilities in the multilayer flow of viscoelastic fluids; Part III. Compatible polymer systems, J. Rheol. 37 (1993) 341.

[8] B. Khomami, G.M. Wilson, An experimental investigation of interfacial instabilities in the superposed flow of viscoelastic fluids in converging/diverging channel geometry, J. Non-Newtonian Fluid Mech. 58 (1995) 47.

[9] H.J. Wilson, J.M. Rallison, Short wave instability of co-extruded elastic liquids with matched viscosities, J. Non-Newtonian Fluid Mech. 72 (1997) 237–251.

[10] H. Ganpule, B. Khomami, A theoretical investigation of interfacial instabilities in the three layer superposed channel flow of viscoelastic fluids, J. Non-Newtonian Fluid Mech. 79 (1998) 315–360.

[11] H. Ganpule, B. Khomami, An investigation of interfacial instabilities in the superposed channel flow of viscoelastic fluids, J. Non-Newtonian Fluid Mech. 81 (1999) 27–69.

[12] S. Scotto, P. Laure, Linear stability of three-layer Poiseuille flow for Oldroyd - B fluids, J. Non-Newtonian Fluid Mech. 83 (1999) 71–92.

[13] R. Valette, P. Laure, Y. Demay, J.F. Agassant, Convective linear stability analysis of two-layer coextrusion flow for molten polymers, J. Non-Newtonian Fluid Mech. 121 (2004) 41–53.

[14] V. Shankar, Stability of two-layer viscoelastic plane Couette flow past a deformable solid layer, J. Non-Newtonian Fluid Mech. 117 (2004) 163–182.

[15] V. Shankar, Stability of two-layer viscoelastic plane Couette flow past a deformable solid layer: implications of fluid viscosity stratification, J. Non-Newtonian Fluid Mech. 125 (2005) 143–158.

[16] R.B. Bird, R.C. Armstrong, O. Hassager, Dynamics of Polymeric Liquids, vol. 1: Fluid Mechanics, John Wiley, New York, 1977.

[17] R.B. Bird, R.C. Armstrong, O. Hassager, Dynamics of Polymeric Liquids, vol. 2: Kinetic Theory, John Wiley, New York, 1977.

[18] L. Landau, E. Lifshitz, Theory of Elasticity, Pergamon, New York, 1989.

[19] O. Kulikov, K. Hornung, A simple way to process surface defects in the processing of polyehtylene, J. Non-Newtonian Fluid Mech. 124 (2004) 103–114.

[20] L.E. Malvern, Introduction to the Mechanics of a Continuous Medium, Prentice-Hall, Englewood Cliffs, NJ, 1969.

[21] C.W. Macosko, Rheology: Principles, Measurements and Applications, VCH, New York, 1994.

[22] R.G. Larson, Constitutive Equations for Polymer Melts and Solutions, Butterworths, Boston, 1988.

[23] R. Sureshkumar, A.N. Beris, R.A. Handler, Direct numerical simulation of turbulent channel flow of a polymer solution, Phys. Fluids 9 (1997) 743–755.

[24] V. Gkanis, S. Kumar, Instability of creeping Couette flow past a neo-Hookean solid, Phys. Fluids 15 (2003) 2864–2871.

[25] V. Gkanis, S. Kumar, Stability of pressure-driven creeping flows in channels lined with a nonlinear elastic solid, J. Fluid Mech. 524 (2005) 357–375.

[26] V. Gkanis, S. Kumar, Instability of gravity-driven free-surface flow past a deformable elastic solid, Phys. Fluids 18 (2006) 044103.

[27] K. Arora, B. Khomami, The influence of finite extensibility on the eigenspectrum of dilute polymeric solutions, J. Non-Newtonian Fluid Mech. 129 (2005) 56–60.

[28] V. Shankar, S. Kumar, Instability of viscoelastic plane Couette flow past a deformable wall, J. Non-Newtonian Fluid Mech. 116 (2004) 371–393.

[29] P. Drazin, W. Reid, Hydrodynamic Stability, Cambridge University Press, Cambridge, 1981.

[30] M. Renardy, Y. Renardy, Linear stability of plane Couette flow of an upper convected Maxwell fluid, J. Non-Newtonian Fluid Mech. 22 (1986) 23–33.